~~CONFIDENTIAL~~

NASA TECHNICAL MEMORANDUM

NASA TM X-1014

NASA TM X-1014

FLOW FIELD AND SURFACE PRESSURES ON A BLUNT HALF-CONE ENTRY CONFIGURATION AT MACH NUMBERS OF 7.4 AND 10.4

by Thomas E. Polek, George H. Holdaway, and Joseph H. Kemp, Jr.

Ames Research Center
Moffett Field, Calif.

NATIONAL AERONAUTICS AND SPACE ADMINISTRATION • WASHINGTON, D. C. • SEPTEMBER 1964

~~CONFIDENTIAL~~

FLOW FIELD AND SURFACE PRESSURES ON A BLUNT HALF-CONE ENTRY CONFIGURATION AT MACH NUMBERS OF 7.4 AND 10.4

By Thomas E. Polek, George H. Holdaway, and Joseph H. Kemp, Jr.

Ames Research Center
Moffett Field, Calif.

NATIONAL AERONAUTICS AND SPACE ADMINISTRATION

FLOW FIELD AND SURFACE PRESSURES ON A BLUNT HALF-CONE ENTRY CONFIGURATION AT MACH NUMBERS OF 7.4 AND 10.4*

By Thomas E. Polek, George H. Holdaway, and Joseph H. Kemp, Jr.

Ames Research Center
Moffett Field, Calif.

SUMMARY

An experimental investigation was made of the flow field and surface pressure distributions for an entry configuration consisting of approximately half of a blunt cone with a semiapex angle of 30° and base-mounted flap-type controls. This configuration commonly known as the M-1 was tested over an angle-of-attack range of -15° to +15° at Mach numbers of 7.4 and 10.4 with corresponding Reynolds numbers based on body length of 800,000 and 600,000.

The results indicate that for some conditions, the body-generated flow field induces high local pressures (coefficients as high as 9.4) and large pressure gradients on the controls. Varying the aspect ratio of the flap caused changes in local flap pressure coefficients of as much as 4.0.

INTRODUCTION

The beneficial effects of lift in decreasing the deceleration and increasing the maneuverability of entry vehicles are discussed in reference 1, and a particular lifting body, referred to as the M-1, was suggested as a possible manned entry configuration. Numerous experimental studies of this shape have been conducted. (The most recent force tests were reported in reference 2, and a list of references to prior investigations may be found in that report.)

In the preliminary investigation of the pressure distribution on the body and controls at Mach numbers from 3 to 6 (ref. 3), unusually large pressure coefficients (up to 5.0) were measured on the control surfaces. Because of the severe heating problem of controls with such large pressure coefficients a more detailed study was made of pressures on and near the controls.

The present report presents the results of this study of pressures on the body and control surfaces and the pitot pressures in the flow field between the shock layer and the body. The study included: (1) effects of control deflection on body surface pressures, (2) effect of aspect ratio on pitch flap pressure distributions, (3) effect of introducing a gap between the base of the model and the flap hinge line on the flap pressure distributions, and (4) interference effects between flap components.

NOTATION

A	aspect ratio, $\frac{\text{width of control}}{\text{length of control}}$
C_p	pressure coefficient, $\frac{p-p_\infty}{q_\infty}$
$C_{p'}$	pitot-pressure coefficient, $\frac{p_p-p_\infty}{q_\infty}$
d	base diameter of model
M	Mach number
p	static pressure
p_∞	free-stream static pressure
p_p	pitot pressure
q_∞	free-stream dynamic pressure
Re	Reynolds number
S	distance measured along a surface element from the point of intersection of the surface with the cone axis
$\overline{S}$	surface distance S at the plane of the base
x	distance from the nose measured parallel to the cone axis
z	distance from the body surface measured parallel to the base plane
α	angle of attack, relative to the flat upper surface of the model
δ	deflection angle of the control[1]
δ_y	deflection angle of the yaw segment of the roll-yaw control[1]
ζ	distance measured normal to the surface
η	angle between the free-stream direction and the normal to the control surface

[1]At zero deflection angle the control is normal to the model base plane for all controls, except the roll control, in which case the deflection angle is zero when the control is in the plane of the side control upon which it is mounted. Positive deflections in all cases are outward into the air stream.

Subscripts

av	average
L	left side looking upstream
l	lower control
max	maximum
R	right side looking upstream
r	roll control
u	upper control

APPARATUS AND TESTS

The tests were conducted in the Ames 3.5-foot hypersonic wind tunnel. This facility is of the blowdown type capable of operating at nominal Mach numbers of 5, 7, and 10, at total pressures up to 1800 pounds per square inch. Stagnation air temperatures up to 2100° R are available for testing times up to 2 minutes. Helium is injected through an annular slot in the subsonic section of the nozzle to provide a layer of cool gas along the nozzle and test section walls. A simplified schematic diagram of the facility and a photograph of the test section are presented in figures 1 and 2. The model support system is hydraulically actuated and servocontrolled over an angle-of-attack range of -5° to +15°. The operation of the wind tunnel is automatic during a test run; the model attitude sequence and the stagnation pressure desired are programmed into the controller prior to a run. The data are recorded on magnetic tape at a rate of 2500 samples per second.

The model was approximately half of a blunt cone with a semiapex angle of 30° and base-mounted flap-type controls. The dimensions of the basic body and the control set investigated are shown in figure 3. The locations of the pressure orifices are given in figures 4 and 5 and representative photographs of the flaps, pressure rakes, and body are shown in figures 6 and 7. The basic control set selected for study consists of single upper and lower pitch flaps having aspect ratios of 1.0 and, for directional control, two side flaps having aspect ratios of 0.6. A quarter segment of each side control was deflected as shown in figures 3(b) and 7(b) to provide roll control in the manner studied in reference 2. These controls are referred to in the manner studied in reference 2. These controls are referred to in this report as "yaw-roll" flaps. The designation 60° - 30°, for instance, will be used to denote $\delta_y = 60°$ with $\delta_r = 30°$. In addition to the basic pitch flaps having an aspect ratio of 1.0, pitch flaps having aspect ratios of 0.6, 0.5, and 0.333 were also tested at deflections of 60° and 90°.

The models were constructed of stainless steel which has good strength at elevated temperatures. Cold air was circulated inside the models to maintain a moderate and invariant temperature of the pressure transducers during the data-taking portion of the test runs.

The tests were conducted at Mach numbers of 7.4 and 10.4 and at full-scale Reynolds numbers, based on the body length, of 800,000 and 600,000, respectively. The data were recorded automatically at each of 14 angle-of-attack positions during an average total testing time of about 1-1/4 minutes. At each angle of attack one of the pressure readings was monitored, and the data were recorded when the pressure stabilized. Since the normal angle-of-attack range for the strut mechanism is -5° to $+15^{\circ}$, it was necessary to test some configurations inverted to cover the $\pm 15^{\circ}$ angle-of-attack range of these tests. A few shadowgraph pictures were taken to indicate the flow pattern for selected configurations.

Three ranges (5, 10, and 50 psia) of strain-gage pressure cells were employed. These were installed so that the range of the cell was capable of measuring the maximum expected pressures at a given location for the tests at a Mach number of 7.4. The estimated maximum errors in the data are listed in the following table:

C_p	Estimated error in C_p and C_p'					
	M = 7.4			M = 10.4		
	50 psia cell	10 psia cell	5 psia cell	50 psia cell	10 psia cell	5 psia cell
8.0	±0.086	- - -	- - -	±0.329	±0.258	- - -
4.0	±.062	±0.032	- - -	±.209	±.138	±0.129
2.0	±.050	±.020	±0.016	±.150	±.078	±.069
.5	±.042	±.011	±.007	±.104	±.033	±.024

In general the data at M = 7.4 repeated within one-half of the above estimated errors.

The maximum estimated error in angle of attack, including possible variations in the free-stream angularity, was $\pm 0.3^{\circ}$.

RESULTS AND DISCUSSION

The measured body surface pressures (in coefficient form) are presented in figure 8. The various results obtained with the controls are presented in figures 9 through 18 and the results of a pitot survey of the flow field near the body are presented in figures 19 through 25. Additional information regarding control aspect-ratio effects is presented in figures 26 through 34.

Contours of constant pressure coefficient, presented in figures 9, 12, 19, 26, and 27, are intended primarily for orientation purposes, since considerable interpolation and extrapolation of experimental data was necessary in the construction of these figures. The spanwise pressure gradients were in general an order of magnitude less than the chordwise pressure gradient on the symmetrical flaps tested (figs. 9, 12, 26, and 27). Hence, only the pressure distribution on the flap center line will be discussed for these flaps.

Body Surface Pressures

Only a sampling of data was taken on the M-1 body without controls. The results, figure 8, are in good agreement with the previous test results of Sarabia, reference 3. For the basic body, estimates based on impact theory agree quite closely with experimental results (fig. 8). The effects of flap deflection on body surface pressures will be discussed in the sections on side flaps and aspect-ratio effects.

Flap Surface Pressures

The pressure coefficients calculated by means of impact theory have been included on the figures with the measured flap-pressure coefficients to indicate the degree of correlation.

Pitch flaps.- The average pressure coefficients on the pitch of flaps, figures 10 and 30, were computed on the basis of equal areas of influence for the pressure measured at each orifice. Computations of the average pressure coefficients were also made from the incremental pitching-moment data of reference 2, with pressure assumed to be uniform on the entire flap. The average pressure coefficients computed by these two methods were in good agreement.

The average pressure coefficients on the lower flap were approximately those estimated by means of impact theory. However, the maximum pressure coefficients on the lower flap were much greater than those predicted. The flow impinging on the flap was compressed by a system of multiple oblique shock waves and, hence, to a higher pressure than possible by a normal shock wave, but the maximum pressure coefficient allowed in impact theory corresponds to the total pressure behind the normal shock.

The discontinuities in maximum pressure coefficient shown in figures 10 and 30 for the same flap deflections relative to the air stream (e. g., $\delta_l + \alpha + 6.6^\circ = 81^\circ$) were the results of differences in the body-induced flow field caused by different body angles of attack.

The slope discontinuities in the maximum pressure coefficient for the 60° and 90° deflected lower flap resulted from not having a pressure orifice

available at the point of $C_{p_{max}}$ for all test conditions. The probable variation of maximum pressure coefficient may be estimated if the pressures measured by the various orifices on the flap are plotted as a function of angle of attack (fig. 11).

The average and maximum pressure coefficients on the upper flap were, in general, lower than those predicted from impact theory. The flow impinging on the flap has been compressed by the bow shock wave, expanded around a corner, and then recompressed by the shock wave ahead of the flap. The stagnation pressure of this flow may be higher or lower than the pressure behind a single normal shock wave, depending on the strengths of the shock waves and the degree of expansion.

Side flap.- The side flap having an aspect ratio of 0.6 is the yaw-roll flap with zero roll deflection of the quarter segment and is the same as the side flap of control set II of reference 3. The correlation of experimental results and impact theory was similar to that of the lower pitch flap. That is, for 30° flap deflections agreement was reasonable while for deflections of 60° and 90° some measured pressure coefficients were extremely high and varied markedly over the control surface. For these cases, as for the lower pitch flap, impact theory is clearly not applicable (fig. 13).

Deflections of the side flap of 60° and 90° caused increases of up to 50 percent in the surface pressure on the body upstream of the flap although all body pressures are small relative to the flap pressures. For the 60° deflected flap this region of increased pressure is near the base of the flap, while for the 90° deflected flap it extends beyond 0.3 of the body length ahead of the flap.

The effect of introducing a gap between the hinge line of the flap and the base of the body, in addition to the slot or gutter shown in figure 3(b), was investigated. The flaps were located 0.013 base diameter from the model base with a gap width of approximately 60 percent of the flap width. The introduction of the gap for the 90° deflected flap caused the bow shock wave to move toward the body and caused higher maximum pressure coefficients as shown in figure 14. As was noted in reference 2, an unsteady motion of the shock wave existed ahead of the flap as normally mounted on the body. Multiple exposure shadowgraphs of the model (fig. 15) show that the introduction of the gap decreases the unsteady motion of the shock wave.

Yaw-roll flaps.- The yaw-roll flaps were tested on both sides of the body such that the rolled quarter segment (figs. 3(b) and 7(b)) was at the top when the flap was mounted on the left side of the body and at the bottom when mounted on the right side. Figures 16 to 18 present the results for the yaw-roll flap. The pressure on the roll segment of the flap is plotted as a function of the relative angle, η, between the stream direction and the normal to the roll segment in figure 16. The figure was plotted in this manner to indicate the large interference effects possible on this type of flap configuration. The pressures measured by the two orifices of the 90° - 90° flap at η near 80° differ because of the pressure gradients in the flow field. These inboard-outboard pressures also differ from those on the 30° - 90° flap

at η near 80° because the angle of attack of the body is different in these two cases with resulting changes in the body flow field. The change in the flow field with angle of attack causes the extreme variation of pressure observed on the 60° - 0° flap.

Examples of the interference effect of the yaw segment of the yaw-roll flap on the roll segment pressure coefficients are illustrated in figure 17. Even though, from the Newtonian flow viewpoint, the roll flap was theoretically shielded, for $\delta_r = 90^\circ$ on the right side pressure coefficients were approximately equal to those at $\delta_r = 0^\circ$.

The interference effect of the roll segment of the flap upon the yaw element is illustrated in figure 18. It may be noted that large deflections of the roll element resulted in large increases in the pressure level on the yaw portion of the flap.

Body Pressure Field

Diagrams of the local pitot pressure coefficient in the flow field about the model in the plane of the base are presented in figure 19. The variation of pressure coefficient for each pitot tube as the angle of attack changes is shown in figure 20. The pitot-pressure-coefficient profiles of the flow field are presented in figures 21 to 25. The pitot pressure rakes were rigidly attached to the base of the model as shown in figure 5 with the probes oriented approximately in the local flow directions when the model was at 0° angle of attack. The pitot pressure coefficients presented have not been corrected for probe misalinement with the local flow.

The movement of the bow shock wave with changes in model attitude may be noted by the steep rise in pressure measured by the pitot pressure tube as it entered the region between the bow shock wave and the body. As the angle of attack was increased, that portion of the bow shock wave which was upstream of the conical lower surface moved away from the body (see fig. 20). This behavior (discussed in ref. 4) is normal for a 30° half-angle cone at this Mach number. The greater apparent bluntness of the bottom surface as the model was pitched to positive angles reduced the peak pressure coefficients over the entire conical surface as shown in figures 21 and 22. The theoretical curves in figure 23 were computed from a blunt-body and method-of-characteristics solution for the flow about a spherically blunted 30° half-angle cone at 0° angle of attack (measured from the cone axis). The data in this figure were measured at a cone angle of attack of 1.6° ($\alpha = -5^\circ$ measured from the model reference plane). The agreement between theory and experiment is quite good.

The low-pressure layer was from 0.1 to 0.2 base diameter thick above the flat upper surface for all angles of attack tested (see figs. 24 and 25). The low-pressure coefficients at $z/d = 0.06$ (fig. 24) are believed to be the result of vortex flow generated at the nose of the model. (See fig. 19.)

Flap Aspect-Ratio Effects on Surface Pressures

The surface-pressure distributions and peak pressures on the pitch flap were strongly influenced by varying the aspect ratio (figs. 26 to 30). The maximum pressure coefficient measured was 9.41 for the lower flap of A = 0.5 deflected 90° with the body at -5° angle of attack. This was considerably higher than the value of 6.35 measured by the pitot rake in the body flow field. The maximum pressure coefficient measured on a 60° deflected flap was 4.94 (fig. 13). The locations of maximum pressure for flaps deflected 60° and 90° were further outboard than that indicated by the pressure rakes, except for the 90° deflected flap at angles of attack greater than 7°. For this case the maximum pressure occurred in the region near the flap hinge line. Comparison of the average pressures shown in figure 31 (obtained by fairing the data presented in figs. 10 and 30) on the flaps of various aspect ratios revealed differences in $C_{p_{av}}$ as great as 1.0, depending on the flap deflection and model angle of attack. Varying the aspect ratio apparently results in a complicated interaction with the body generated flow field and, hence, no general conclusion seems possible without considerably more knowledge of the complex flows that result from these interactions.

A 60° deflection of the lower flap of aspect ratio 1.0 increased the pressure coefficient on the conical surface of the body in the region of the base of flap by as much as 0.4, but no effect was noted for the flaps of lower aspect ratio (fig. 32(b)). For the 90° deflected lower flap, in the angle-of-attack range from -5° to +5°, the high pressure region on the surface of the body in the region of the base moves upstream as the aspect ratio is increased. This behavior would be expected for a separated flow region at the base of the flap; however, no explanation is offered for the apparent decrease in pressure near the base of the flap ($S/\overline{S}$ = 1.0) for the flaps of higher aspect ratio. In the angle-of-attack range from 10° to 15°, the separated region and associated higher pressures on the body surface moved slightly upstream as the aspect ratio increased. The surface pressures upstream of the upper pitch flap were increased only when the flap was deflected 90°, for aspect ratios equal to or greater than 0.5, and the model angle of attack was less than about 10° (see fig. 33).

Providing a gap between the base of the body and the hinge line of the flap generally increased the pressure gradients on the flap and reduced the unsteady movement of the shock wave upstream of the flap.

SUMMARY OF RESULTS

An experimental investigation of the M-1 entry configuration at Mach numbers of 7.4 and 10.4, at Reynolds numbers of 800,000 and 600,000, respectively, has been made to determine the pressure distributions on various controls, and the layer between the bow wave and the body. The effects of aspect ratio on flap pressure distribution, the effect of flap deflection

and flap aspect ratio on body surface pressures, and the effect on flap pressure distribution of a gap between the base of the body and hinge line of the flap were also investigated.

The local pressures on the base-mounted, flap-type controls were strongly influenced by the flow field generated by the body, and pressure coefficients as high as 9.41 were measured on the 90° deflected flaps. For flap deflections limited to 60°, however, the maximum measured pressure coefficient was 4.94. For compound flap controls, such as the yaw-roll controls tested, the mutual interference effects between the control segments became quite noticeable.

Varying the aspect ratio of the flaps did not produce consistent results for the two flap deflection angles (60° and 90°) tested. At the same deflection angles and at the same angles of attack, varying the aspect ratio of the flaps caused changes in local surface-pressure coefficient of as much as 4.7.

The effect of flap deflection upon body surface pressures was negligible beyond 0.2 of the flap-to-stagnation-point distance upstream from the flap for all of the flaps tested up to 60° deflection. The largest increases in pressure coefficient on the body were 0.4 for the lower flap deflected 60° and 0.8 for a 90° deflection.

Providing a gap between the base of the body and the hinge line of the flap generally caused greater pressure gradients on the flap and reduced the unsteady movement of the shock wave upstream of the flap.

Ames Research Center
National Aeronautics and Space Administration
Moffett Field, Calif., June 18, 1964

REFERENCES

1. Eggers, Alfred J., Jr., and Wong, Thomas J.: Re-entry and Recovery of Near-Earth Satellites, With Particular Attention to a Manned Vehicle. NASA MEMO 10-2-58A, 1958.

2. Holdaway, George H., Polek, Thomas E., and Kemp, Joseph H., Jr.: Aerodynamic Characteristics of a Blunt Half-Cone Entry Configuration at Mach Numbers of 5.2, 7.4, and 10.4. NASA TM X-782, 1963.

3. Sarabia, Michael F.: Aerodynamic Characteristics of a Blunt Half-Cone Entry Configuration at Mach Numbers From 3 to 6. NASA TM X-393, 1960.

4. Greenberg, Robert A., and Traugott, Stephan C.: Shock Wave Asymmetry for Cones and Sphere Cones at Angle of Attack. ARS Jour., June 1961, pp. 821-2.

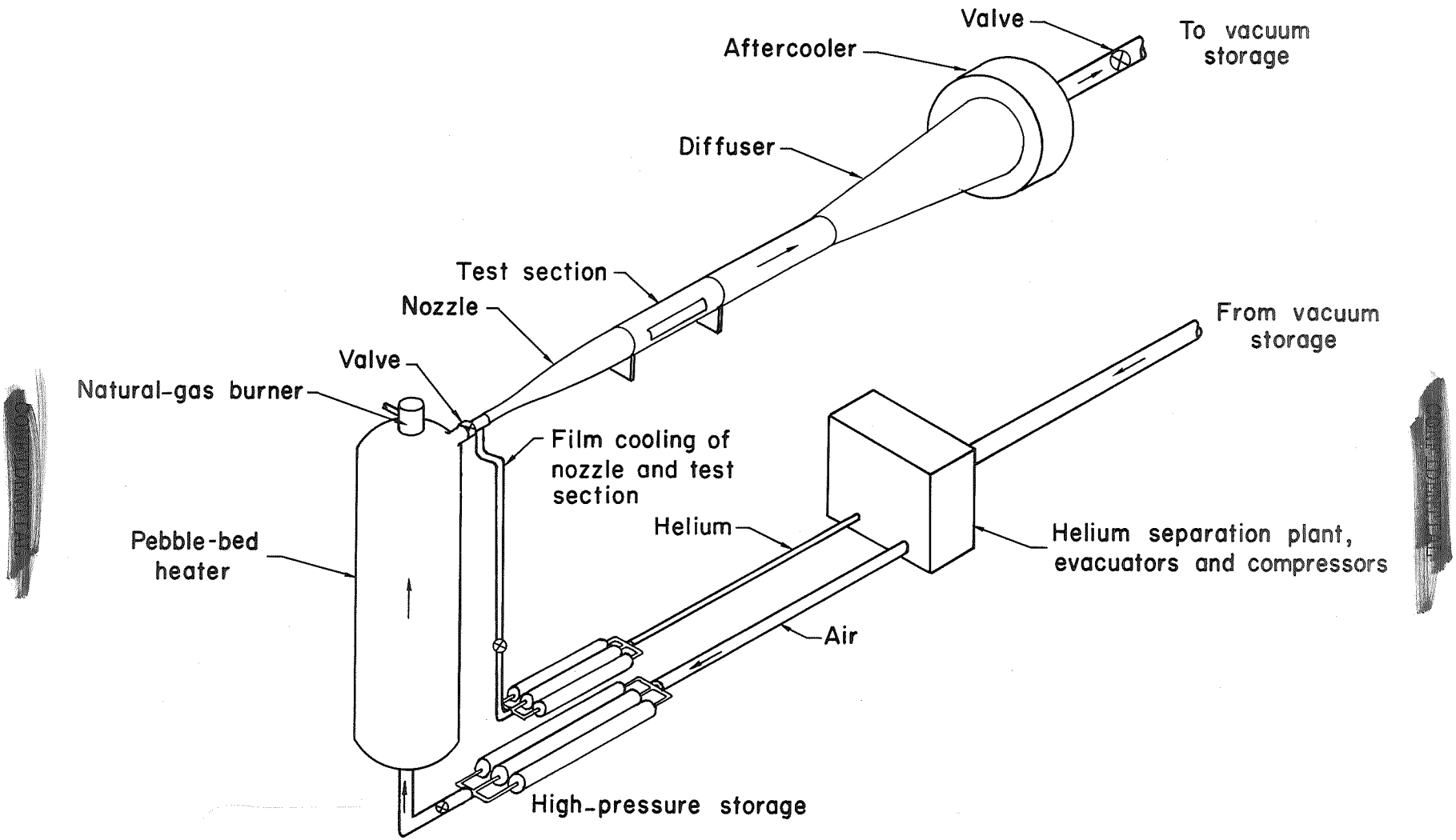

Figure 1.- Schematic sketch of the 3.5-foot hypersonic wind tunnel.

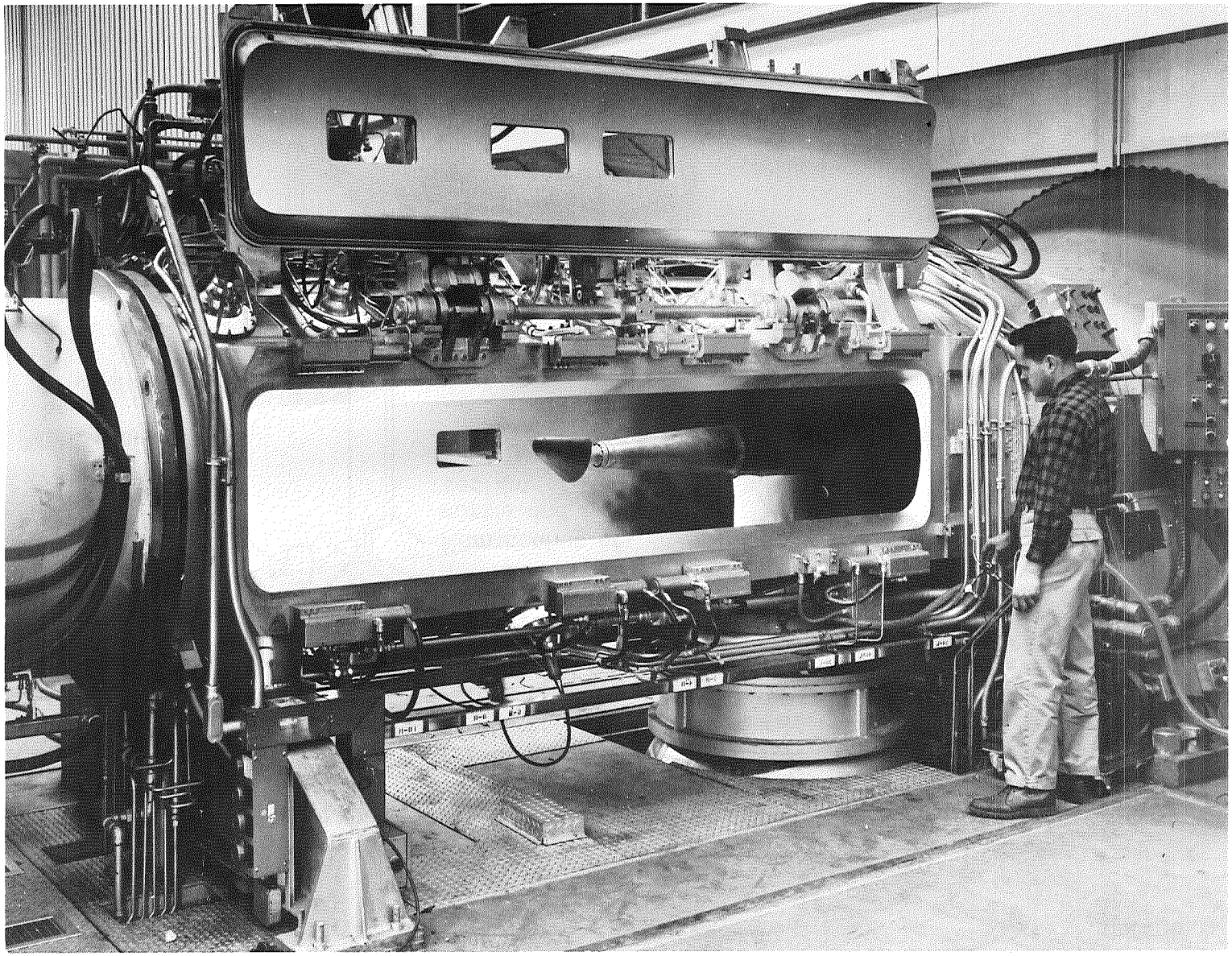

A-29008

Figure 2.- Test section of the Ames 3.5-foot hypersonic wind tunnel.

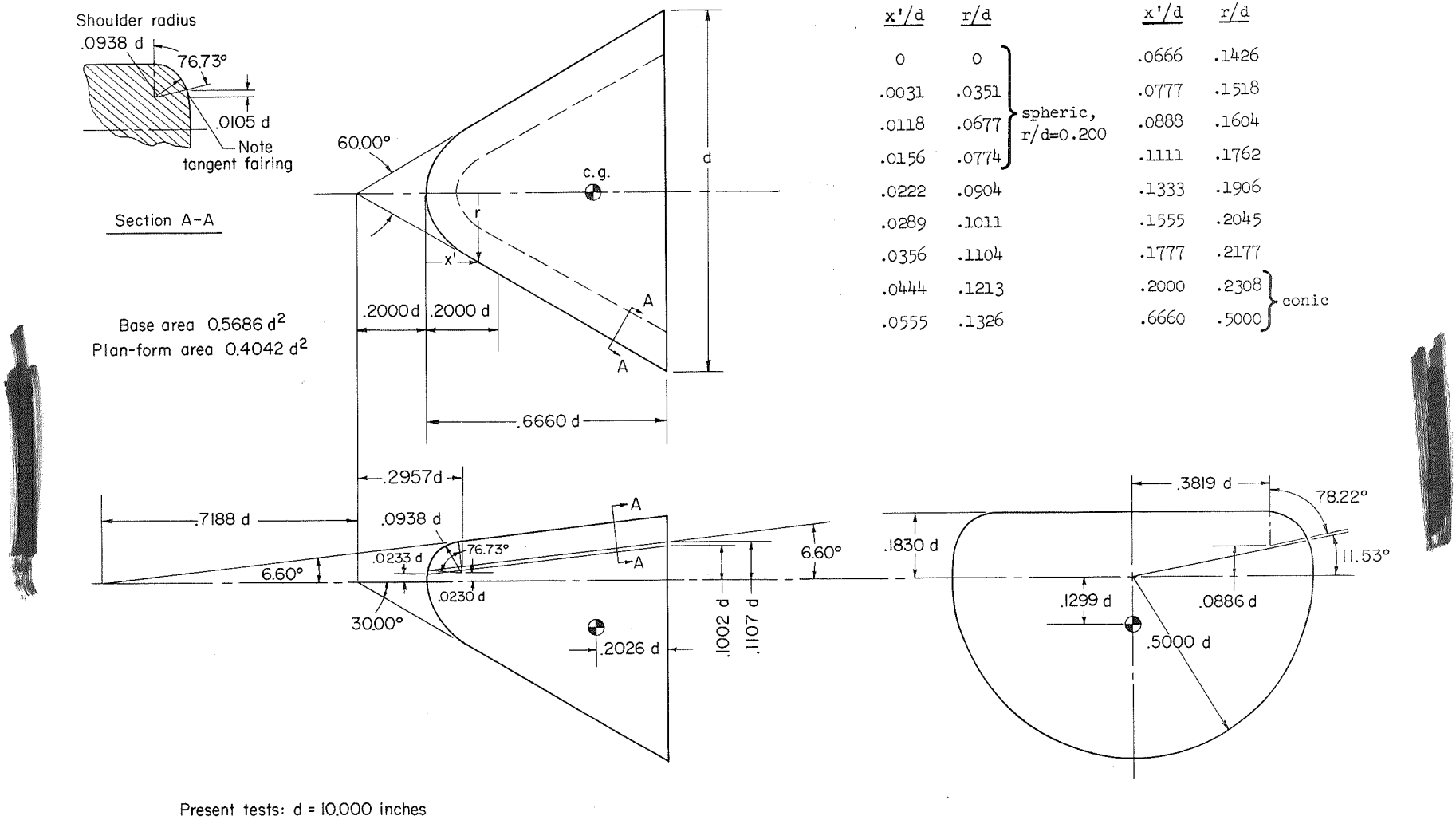

x'/d	r/d		x'/d	r/d	
0	0	spheric, r/d=0.200	.0666	.1426	
.0031	.0351		.0777	.1518	
.0118	.0677		.0888	.1604	
.0156	.0774		.1111	.1762	
.0222	.0904		.1333	.1906	
.0289	.1011		.1555	.2045	
.0356	.1104		.1777	.2177	
.0444	.1213		.2000	.2308	conic
.0555	.1326		.6660	.5000	conic

(a) M-1 body.

Figure 3.- Dimensions of the basic body and control set II.

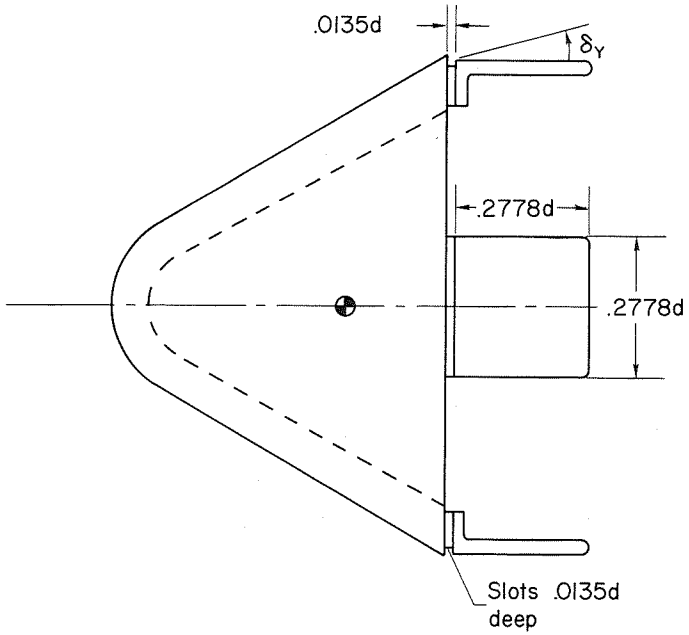

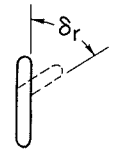

Section B – B

Present tests: d = 10.000 inches

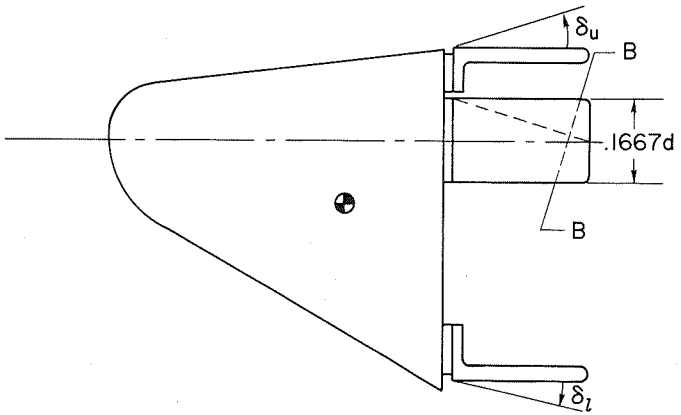

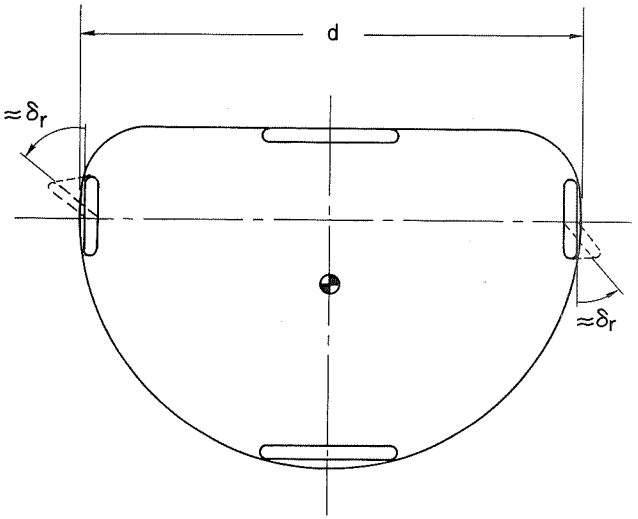

(b) Control set II.

Figure 3.- Concluded.

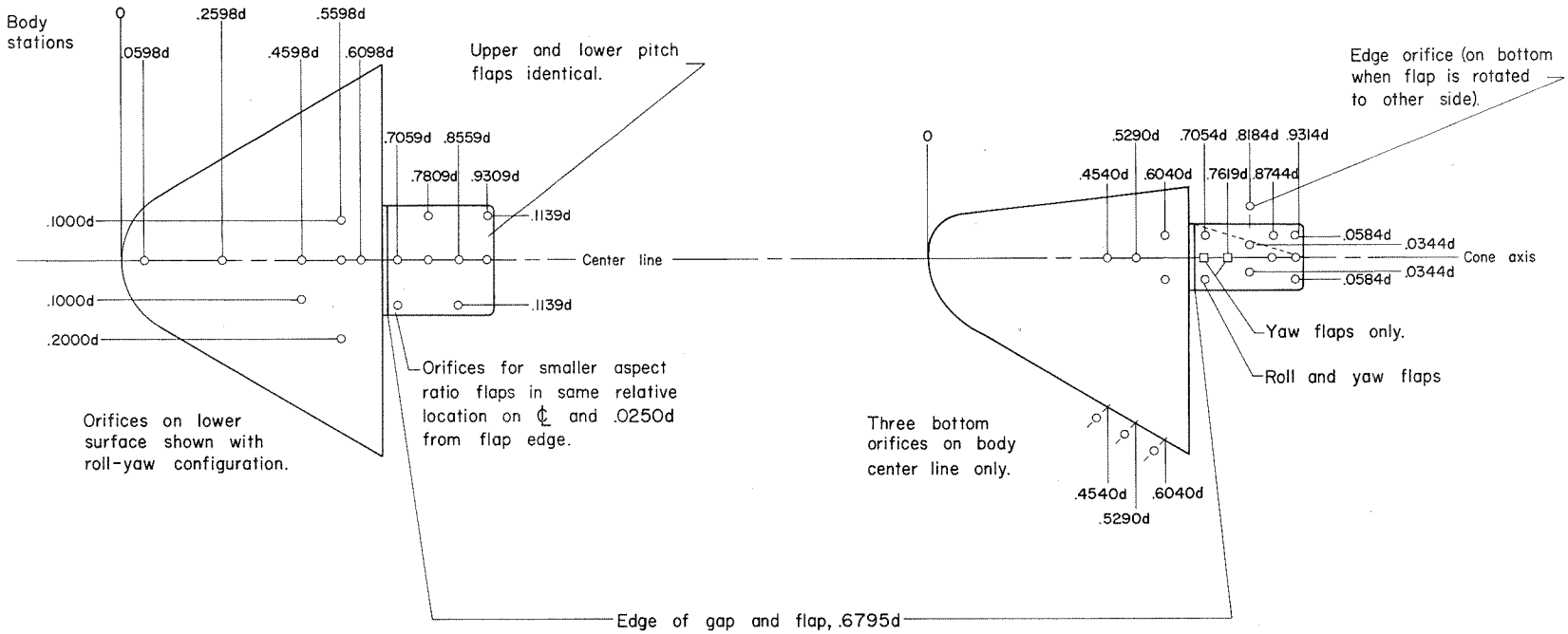

Figure 4.- Location of pressure orifices on the body and flaps.

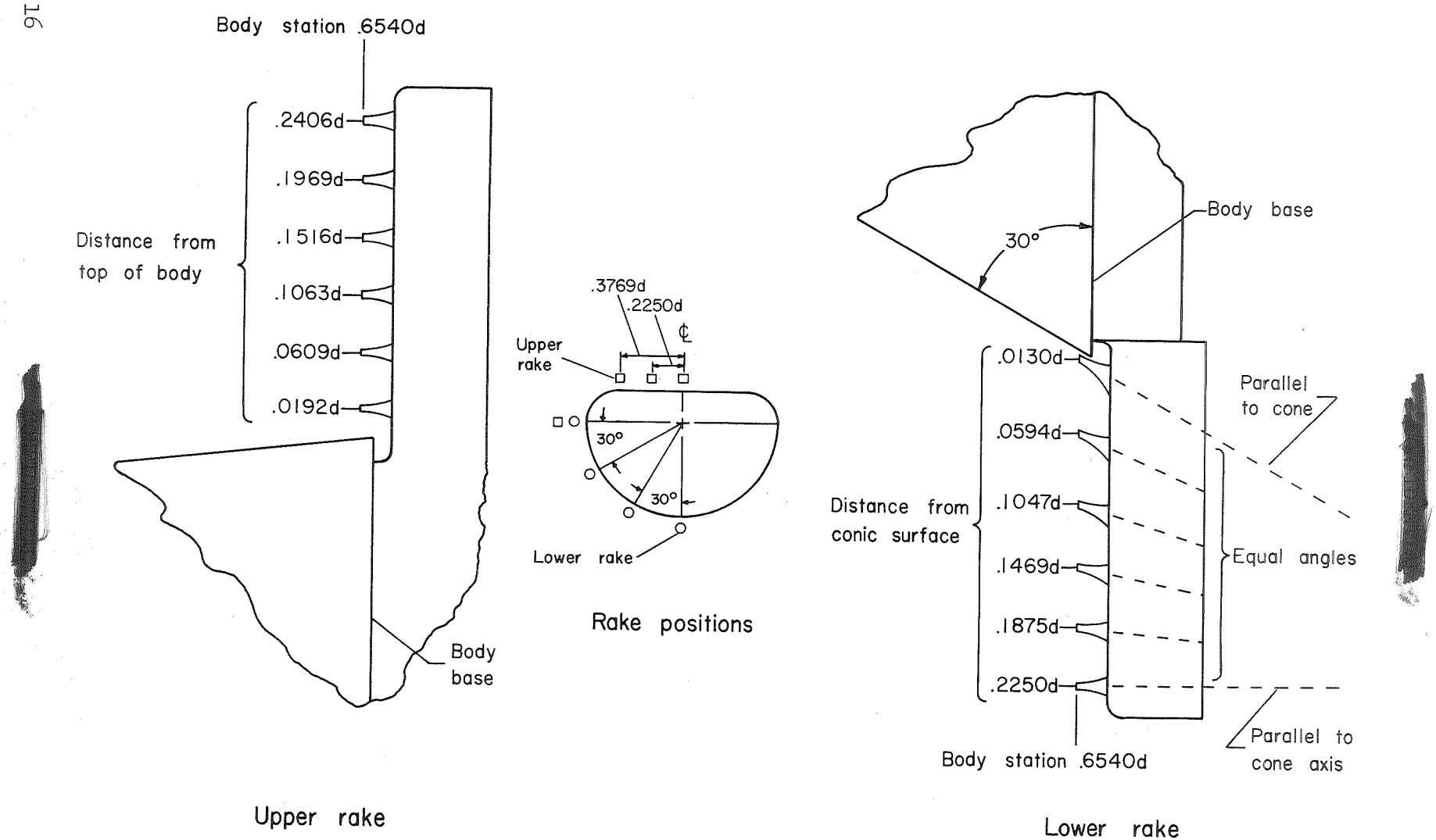

Figure 5.- Location of pressure rakes near the base of the body.

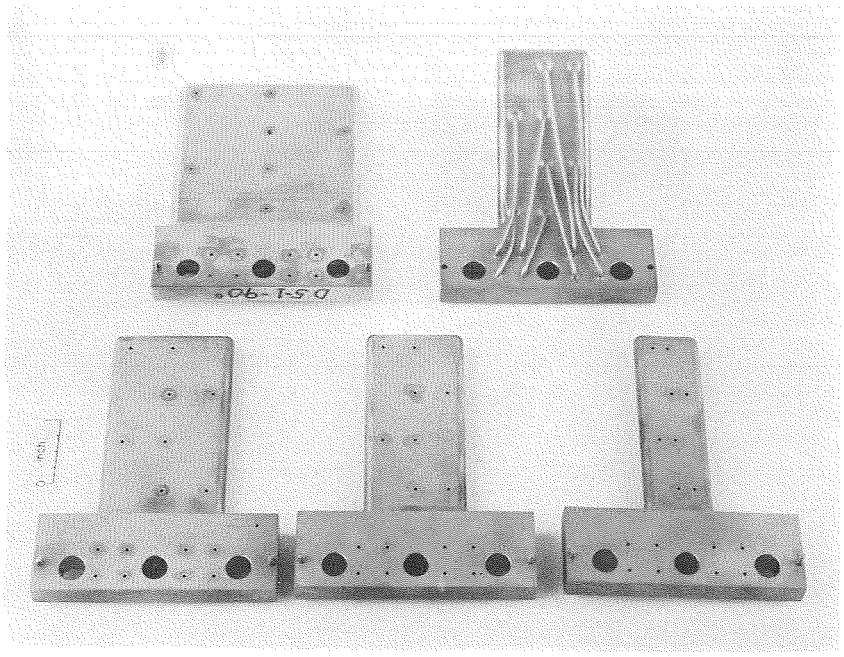

A-28551

(a) $\delta = 90^{\circ}$ pitch flaps (A = 1.0, 0.6, 0.5, and 0.333) and the back of the $\delta = 60^{\circ}$ pitch flap (A = 0.5).

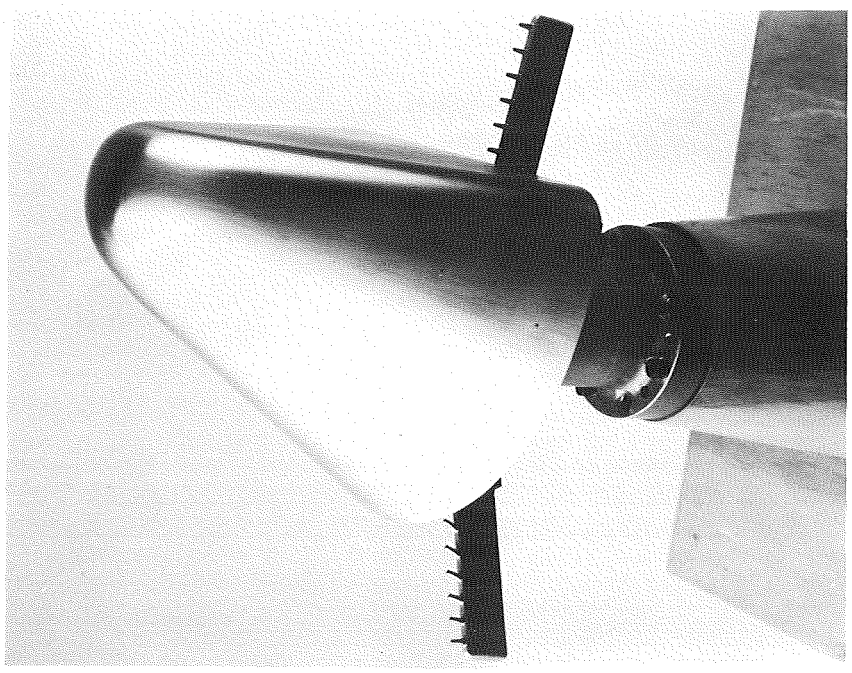

A-28552

(b) Upper and lower pressure rakes.

Figure 6.- Representative pitch flaps of different aspect ratios and the pressure rakes in an off center-line position.

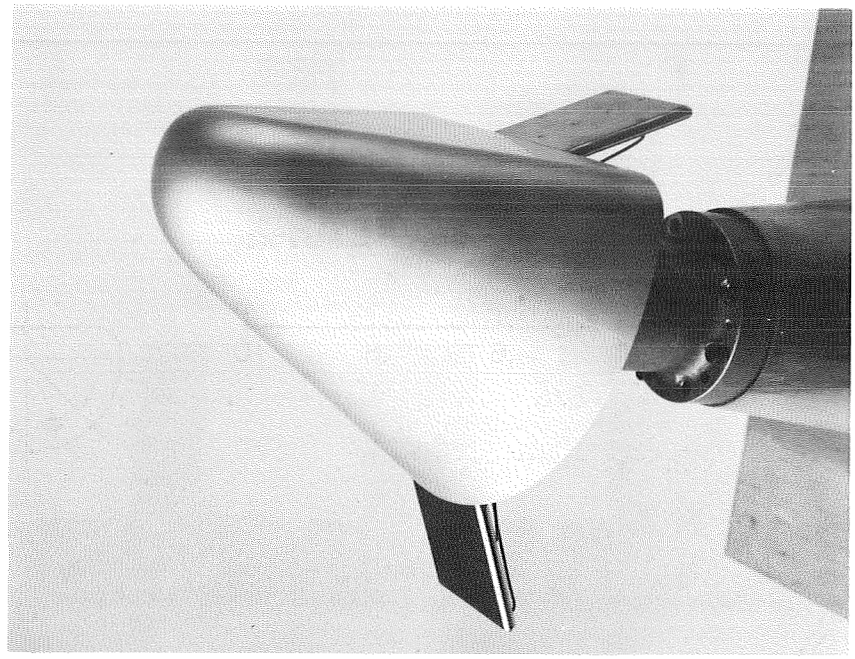

A-28549

(a) Test configuration with two pitch flaps.

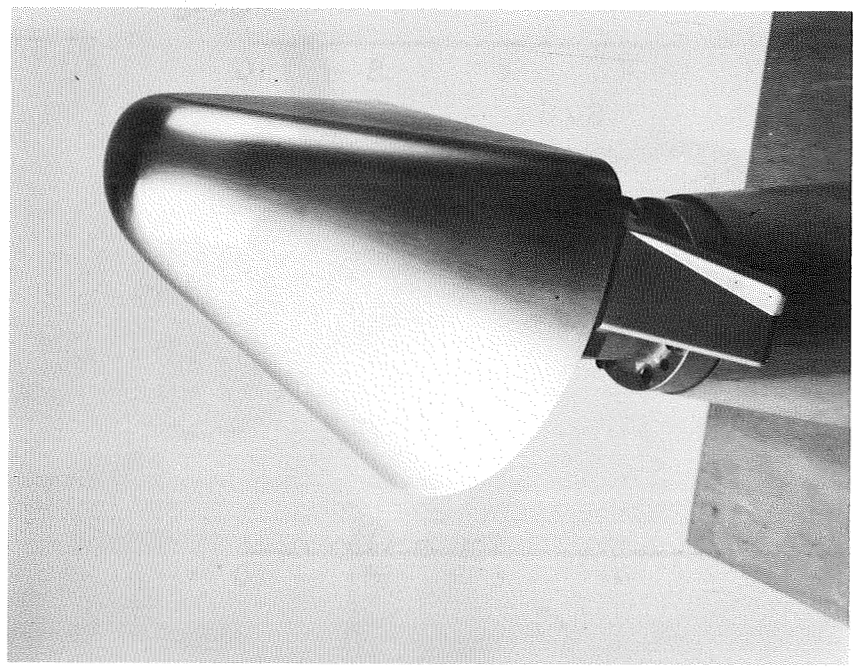

A-28550

(b) Test configuration with yaw-roll flaps.

Figure 7.- Representative test configurations.

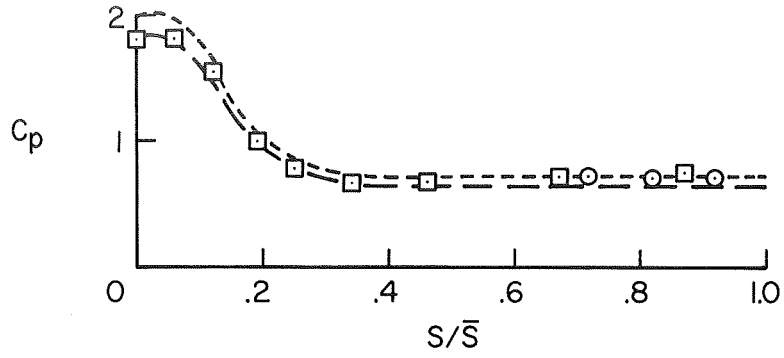

(a) Conical surface, $\varphi = 0^\circ$.

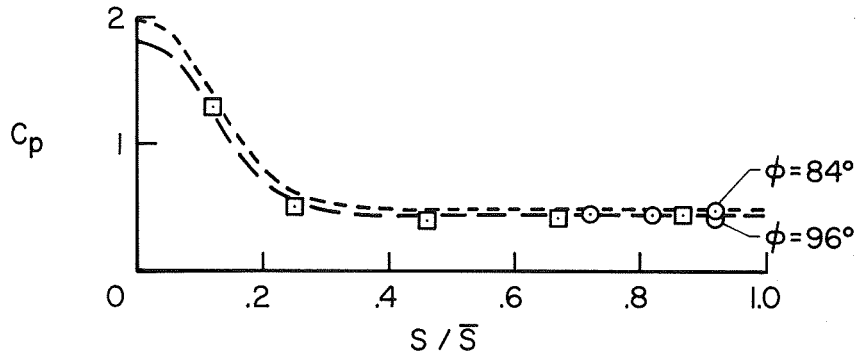

(b) Conical surface, $\varphi = 90^\circ$.

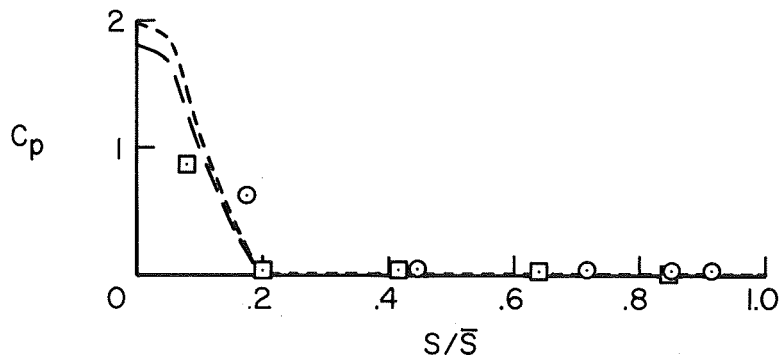

(c) Flat upper surface, $\varphi = 180^\circ$.

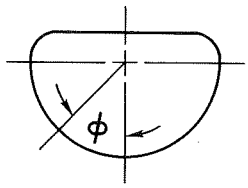

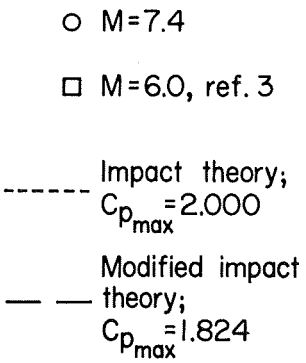

Figure 8.- Pressure-coefficient distribution on the basic M-1 body at $\alpha = 0^\circ$ and M = 7.4.

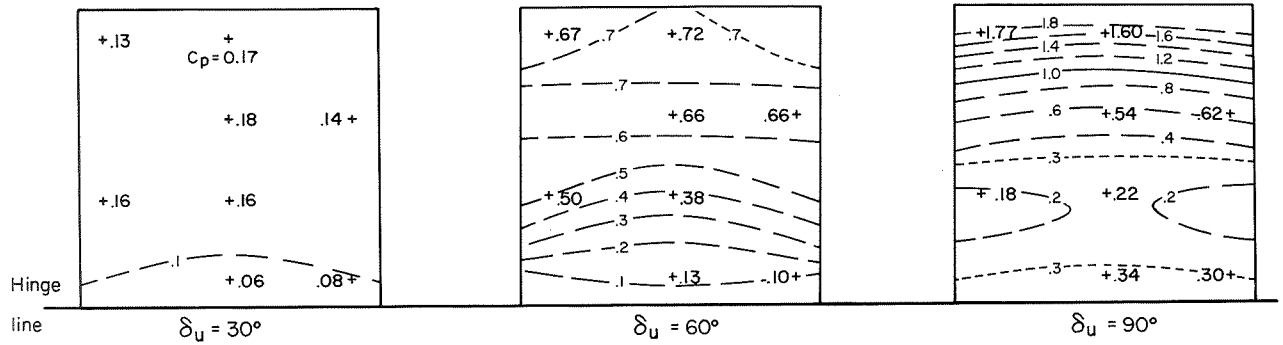

(a) Upper pitch flap.

Unit pressure
Fraction pressure
Uncertain pressure

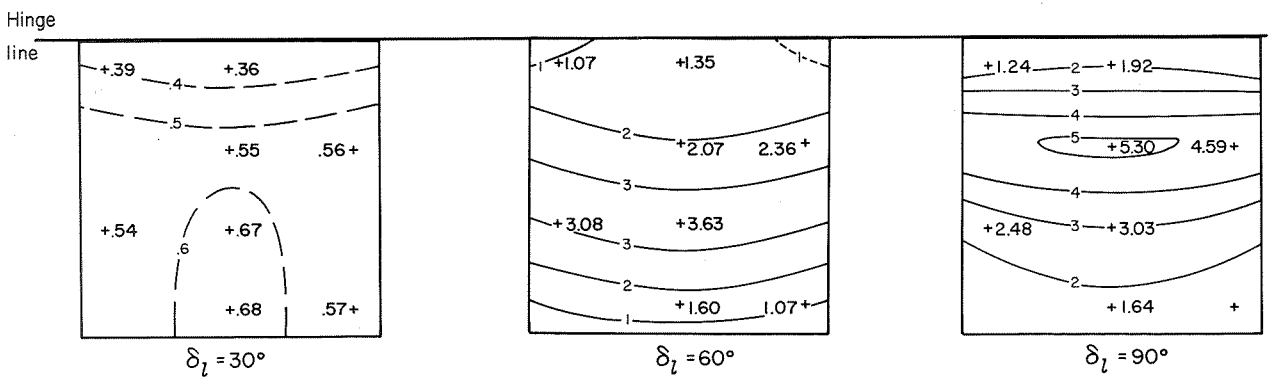

(b) Lower pitch flap.

Figure 9.- Isobar diagrams of pressure-coefficient distributions on A = 1.0 flaps for various deflections at $\alpha = 0^{\circ}$ and M = 7.4.

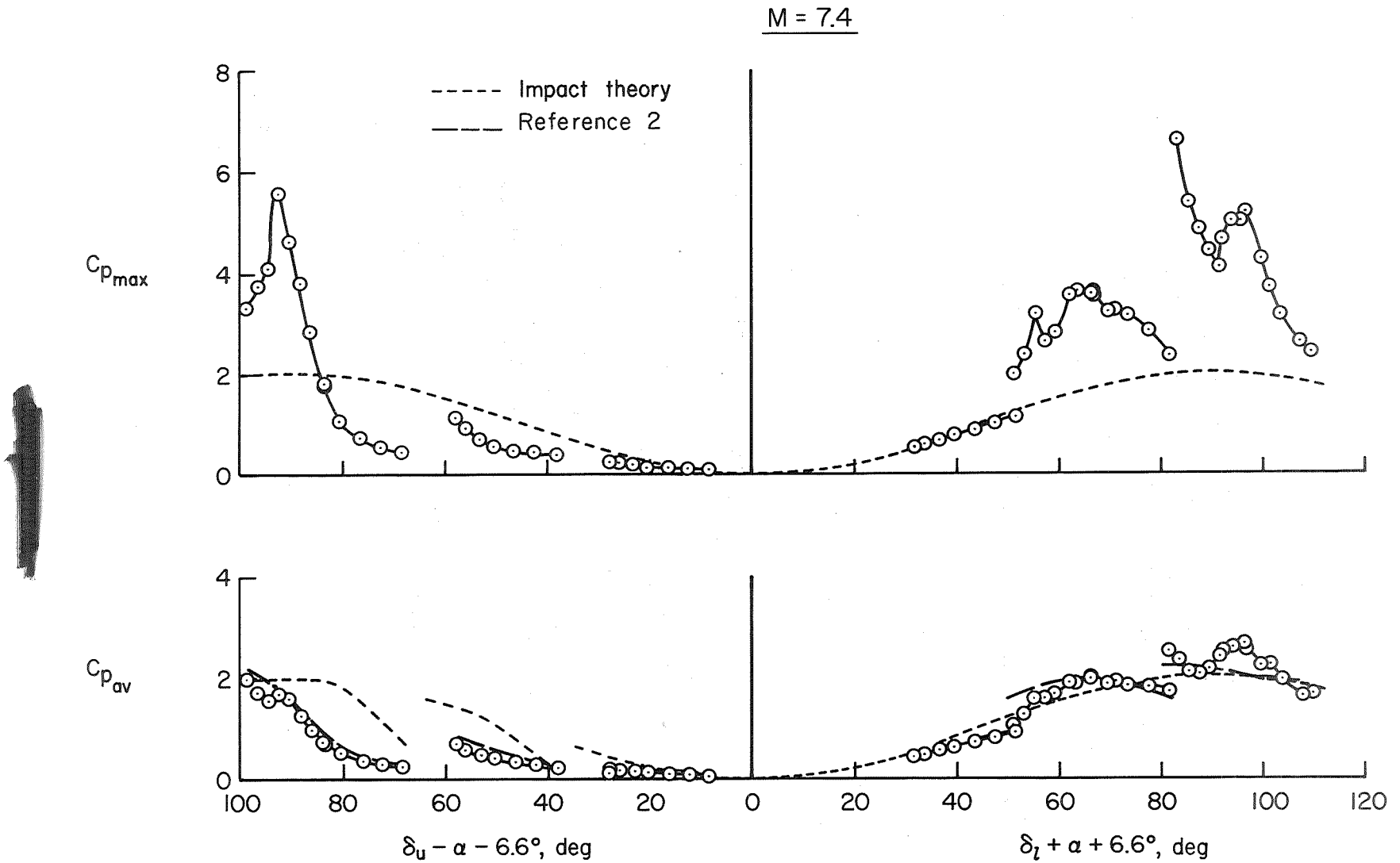

Figure 10.- Maximum and average pressure coefficients on upper and lower pitch flaps (A = 1) as a function of the angle between the free stream and the flap at M = 7.4.

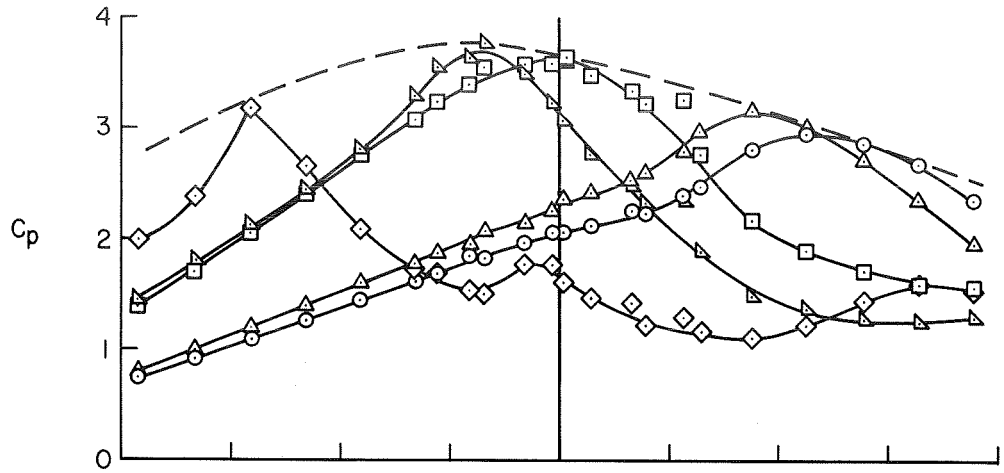

(a) $\delta_l = 60^\circ$, A = 1.0

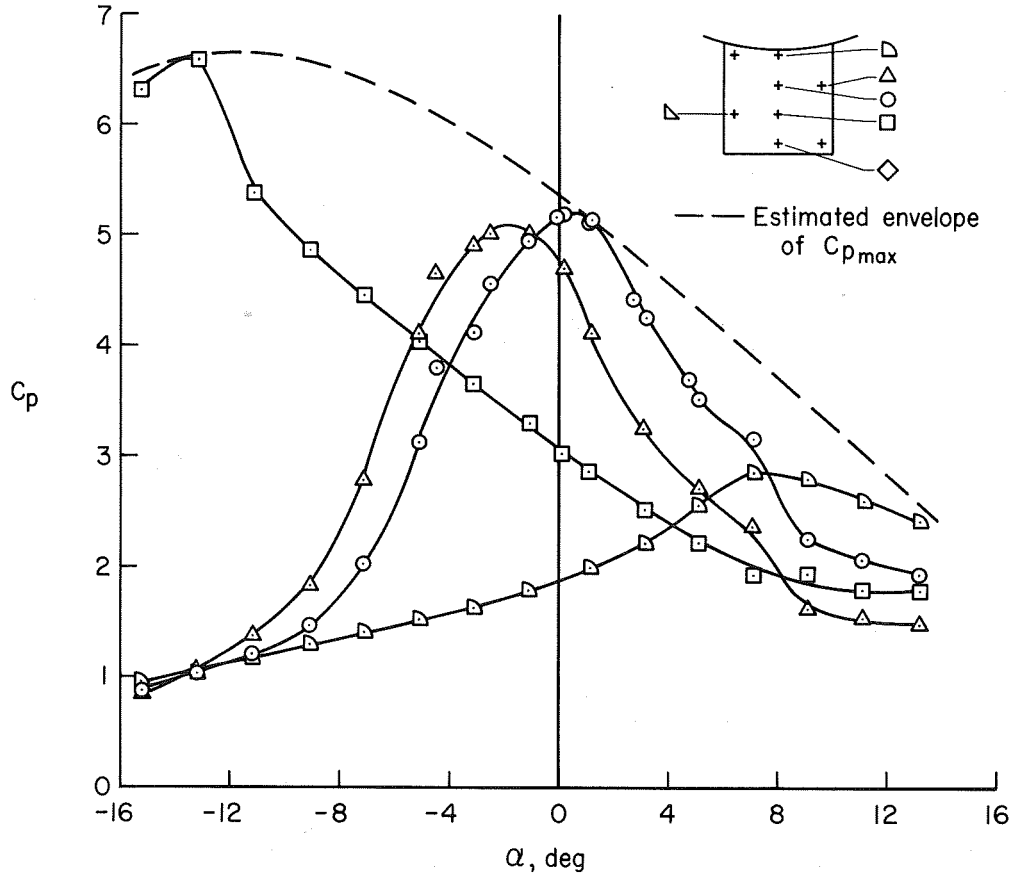

(b) $\delta_l = 90^\circ$, A = 1.0

Figure 11.- Variation of pressure coefficient with angle of attack on selected pitch flaps at M = 7.4.

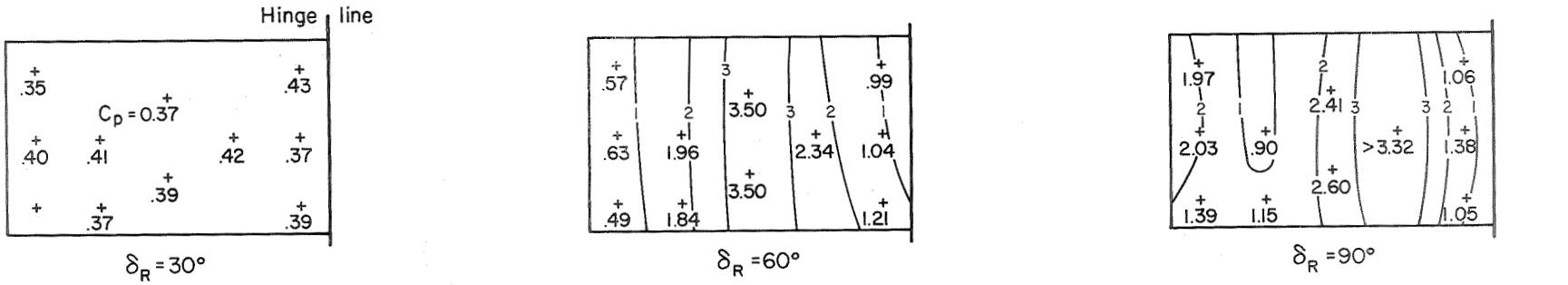

(a) M = 7.4

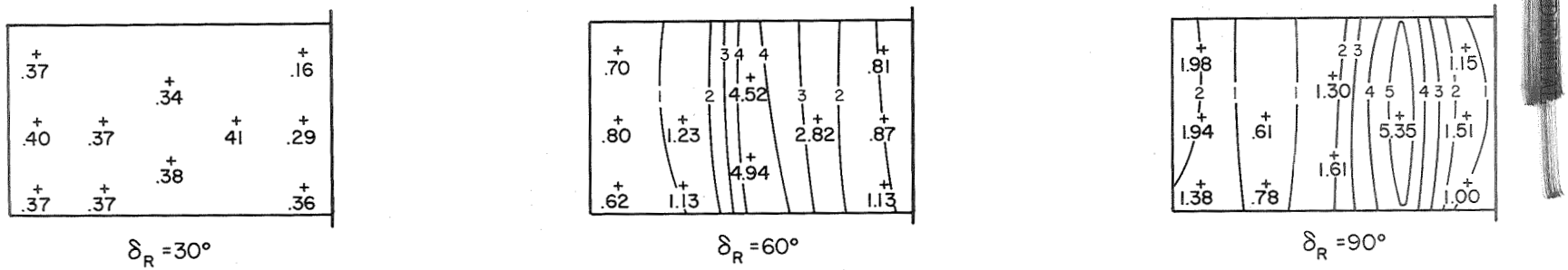

(b) M = 10.4

Figure 12.- Isobar diagrams of pressure-coefficient distributions on right-side flap for various deflections at $\alpha = 0^{\circ}$.

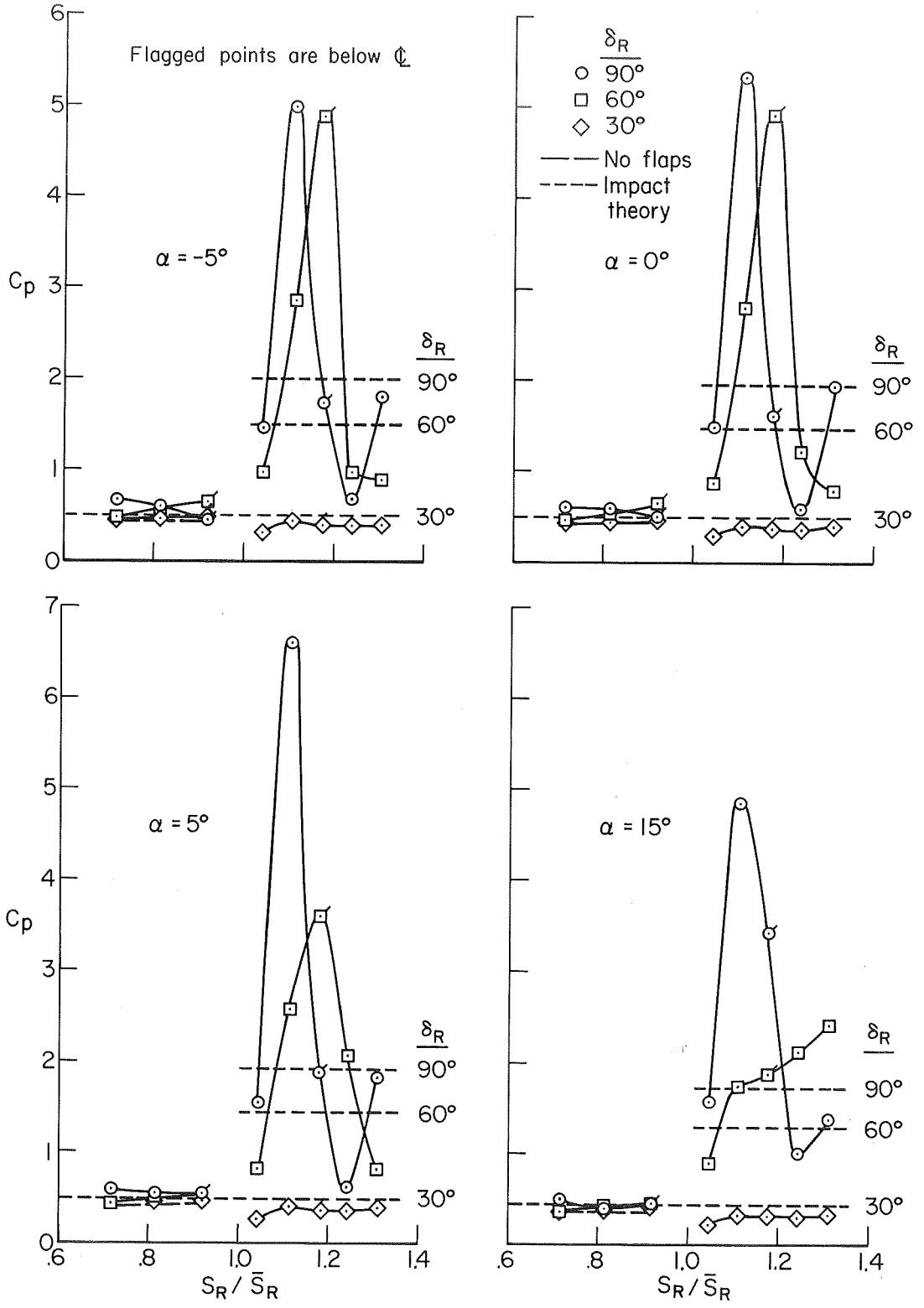

Figure 13.- Pressure-coefficient distributions along the body and the center line of the right-side flap (A = 0.6) at M = 10.4.

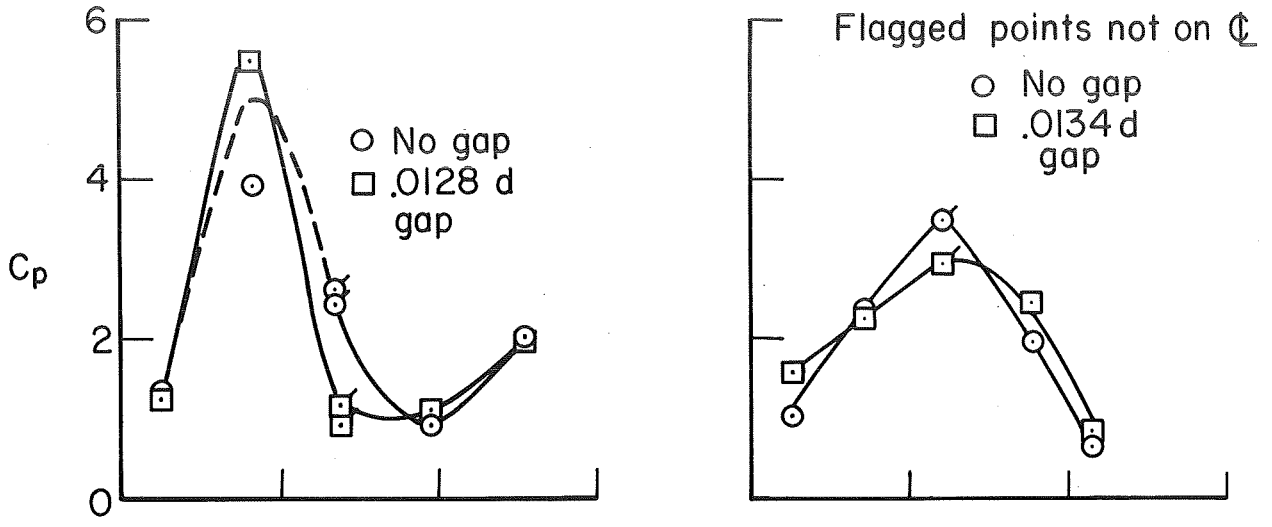

(a) M = 7.4

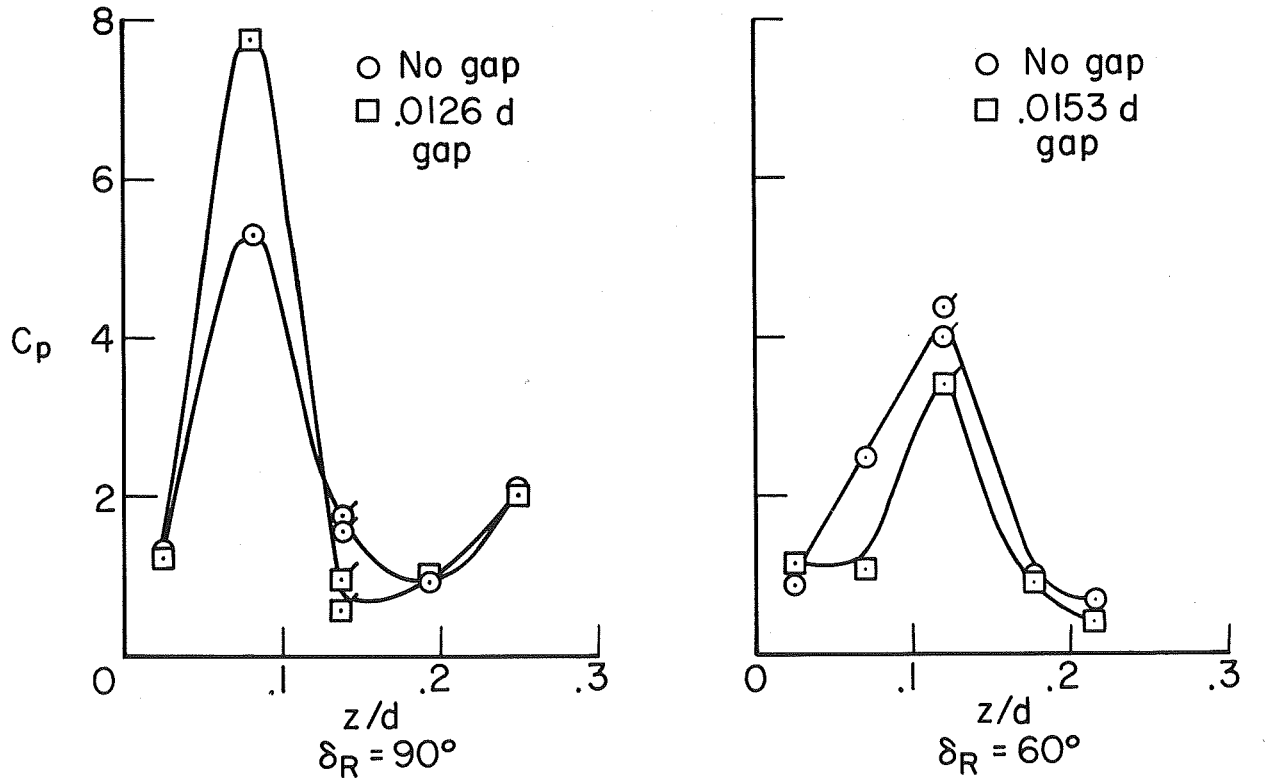

(b) M = 10.4

Figure 14.- Effect of gap on pressure-coefficient distribution along the center line of the side flap at $\alpha = 0^{\circ}$.

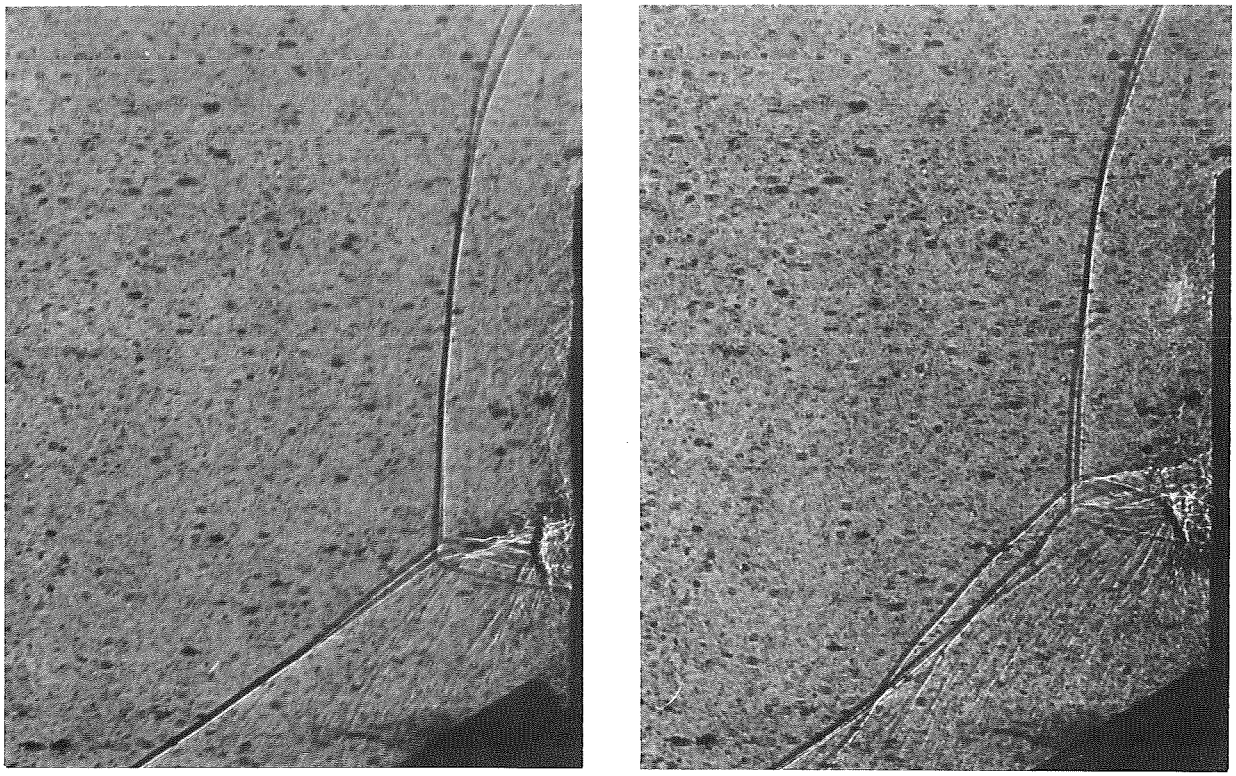

0.141-inch gap. No gap.

Figure 15.- Effect of gap on the unsteady location of shock waves for the right side flap, $\delta_R = 90^\circ$ and $\alpha = 0^\circ$, at $M = 7.4$.

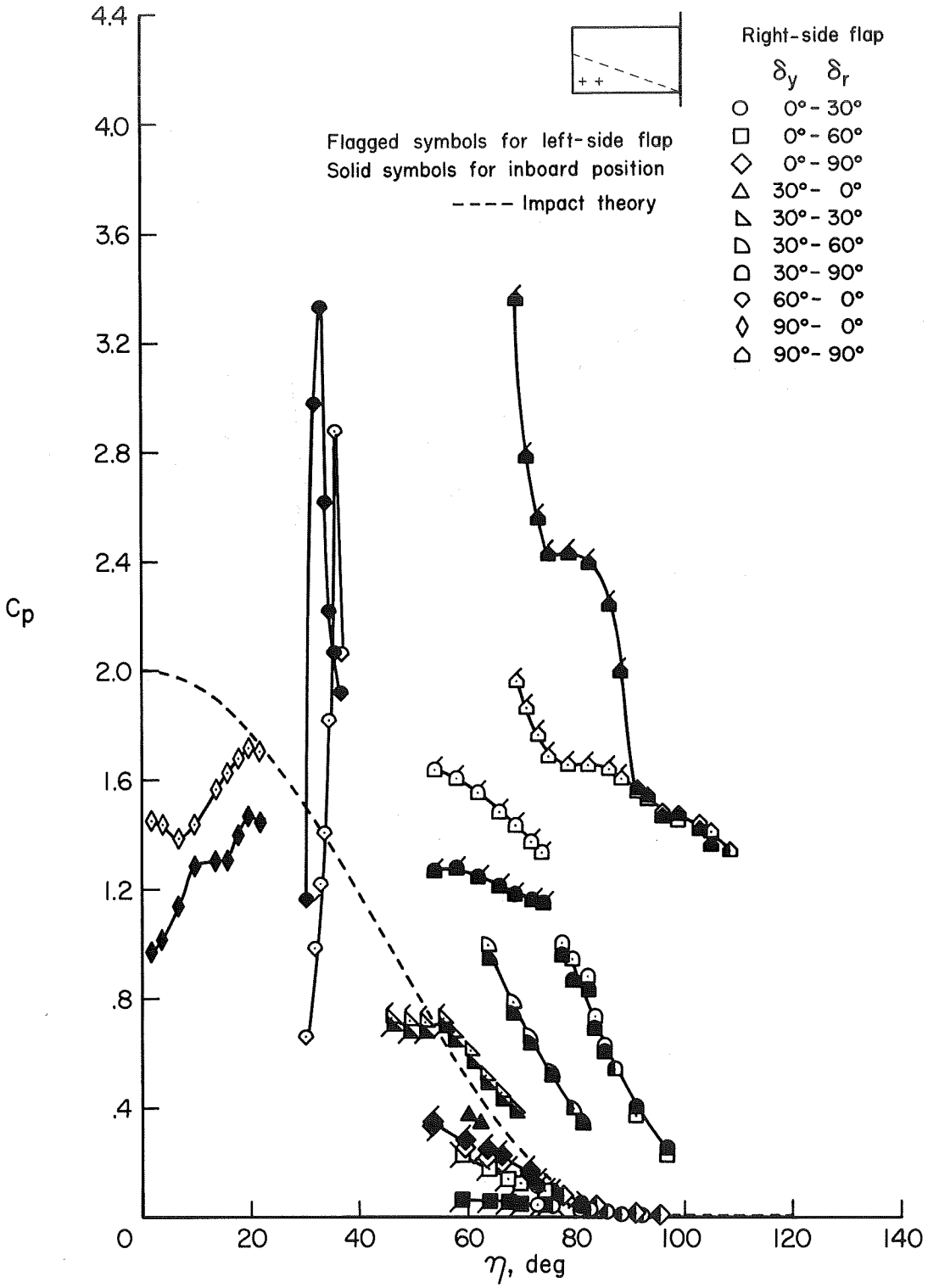

Figure 16.- Pressure coefficient on the roll-flap segment versus the angle between the free-stream direction and the normal to the roll segment at M = 7.4.

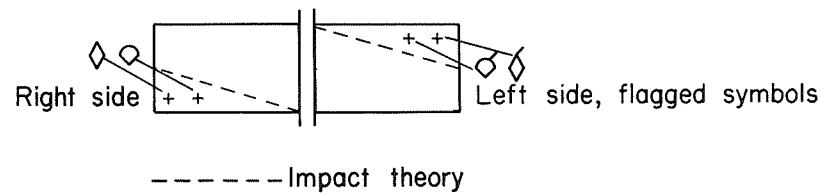

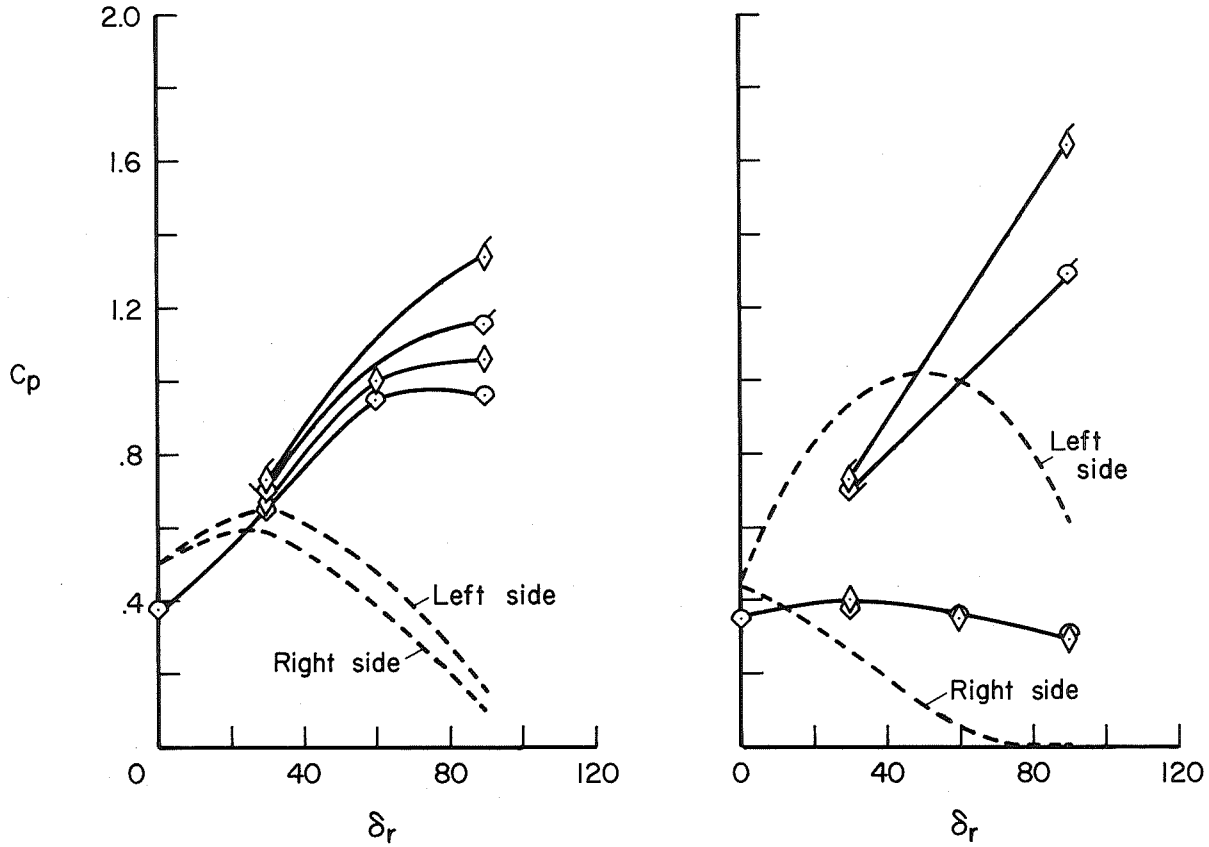

(a) $\alpha = -5^\circ$ (b) $\alpha = 13^\circ$

Figure 17.- Pressure on the roll segment of the yaw-roll flap versus roll-flap deflection for δ_{y_L} and $\delta_{y_R} = 30^\circ$ at M = 7.4.

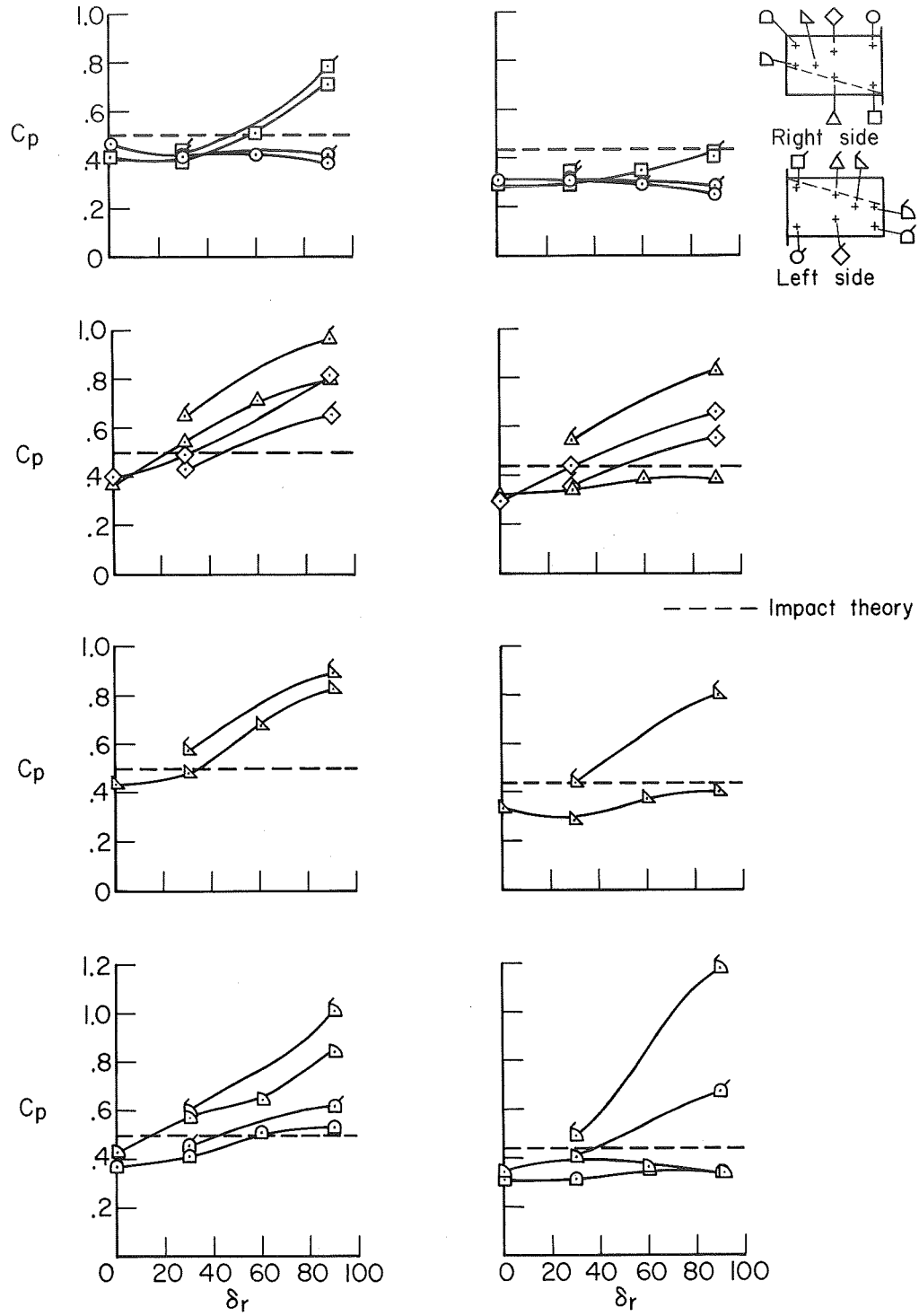

Figure 18.- Pressure-coefficient distribution on yaw segment of yaw-roll flap as a function of roll-flap deflection for δ_{y_L} and δ_{y_R} = 30° at M = 7.4.

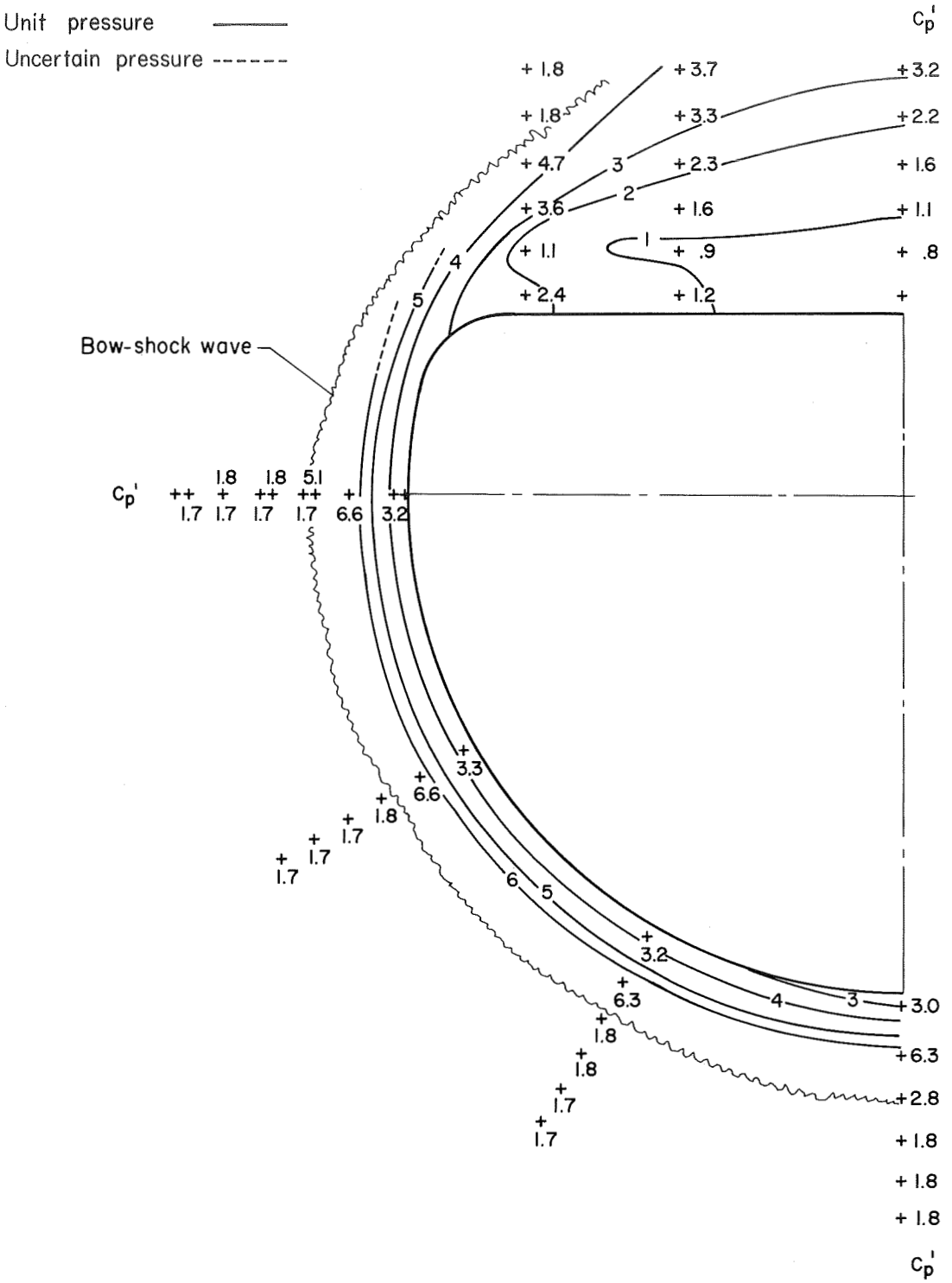

(a) $\alpha = -5^{\circ}$

Figure 19.- Pitot-pressure-coefficient diagram of the flow field about the M-1 body at M = 7.4.

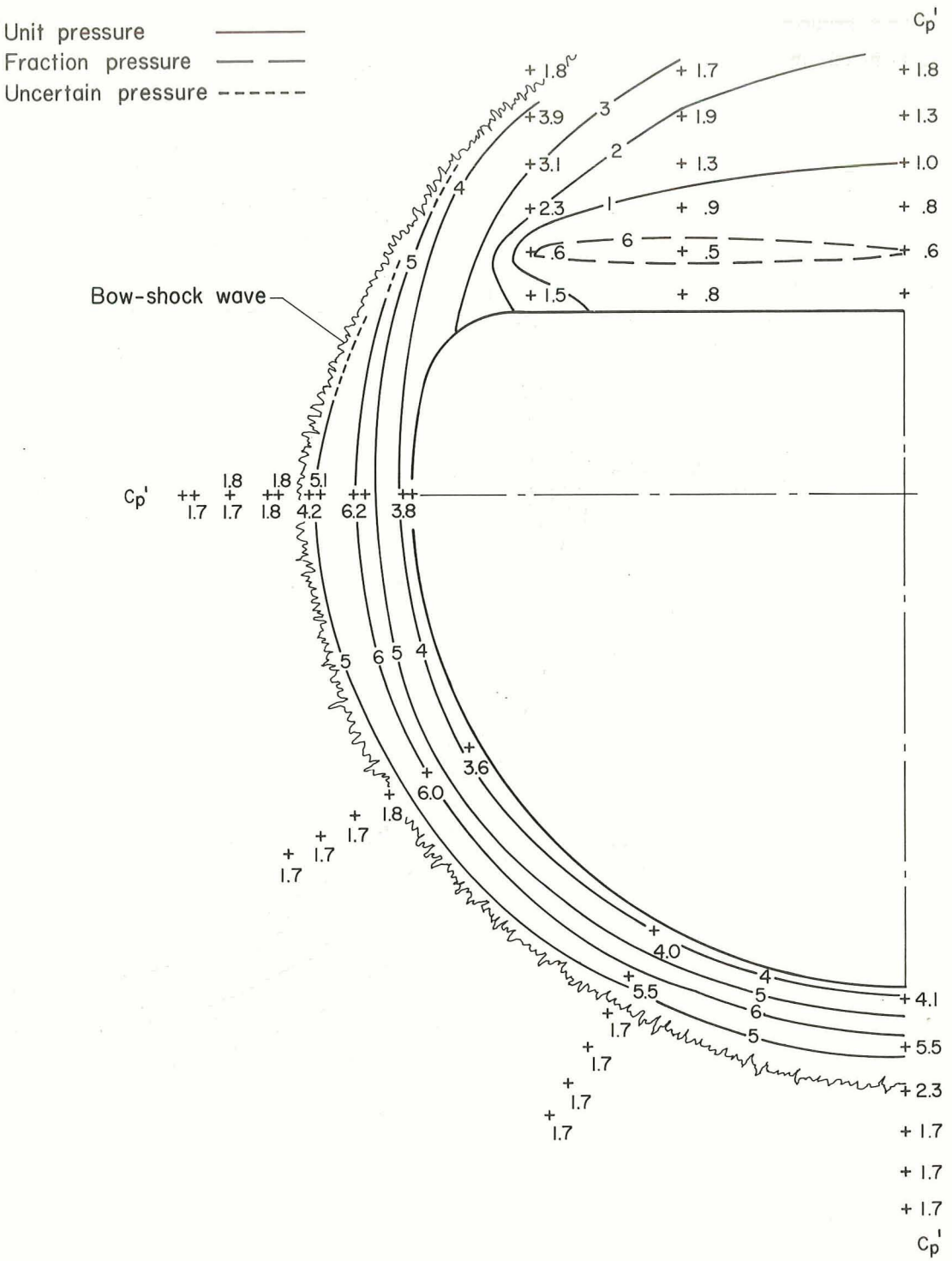

(b) $\alpha = 0^{\circ}$

Figure 19.- Continued.

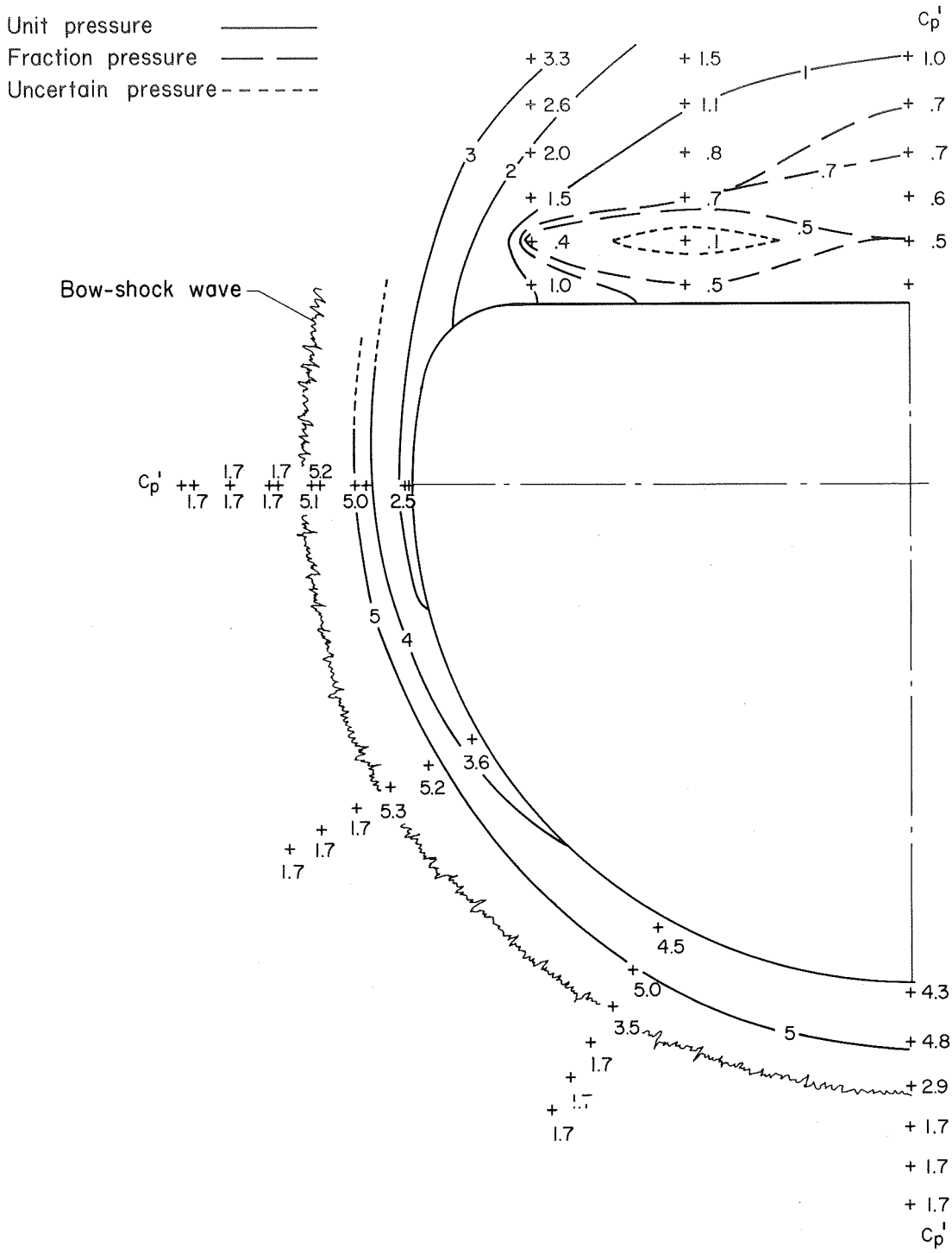

(c) $\alpha = 5^{\circ}$

Figure 19.- Continued.

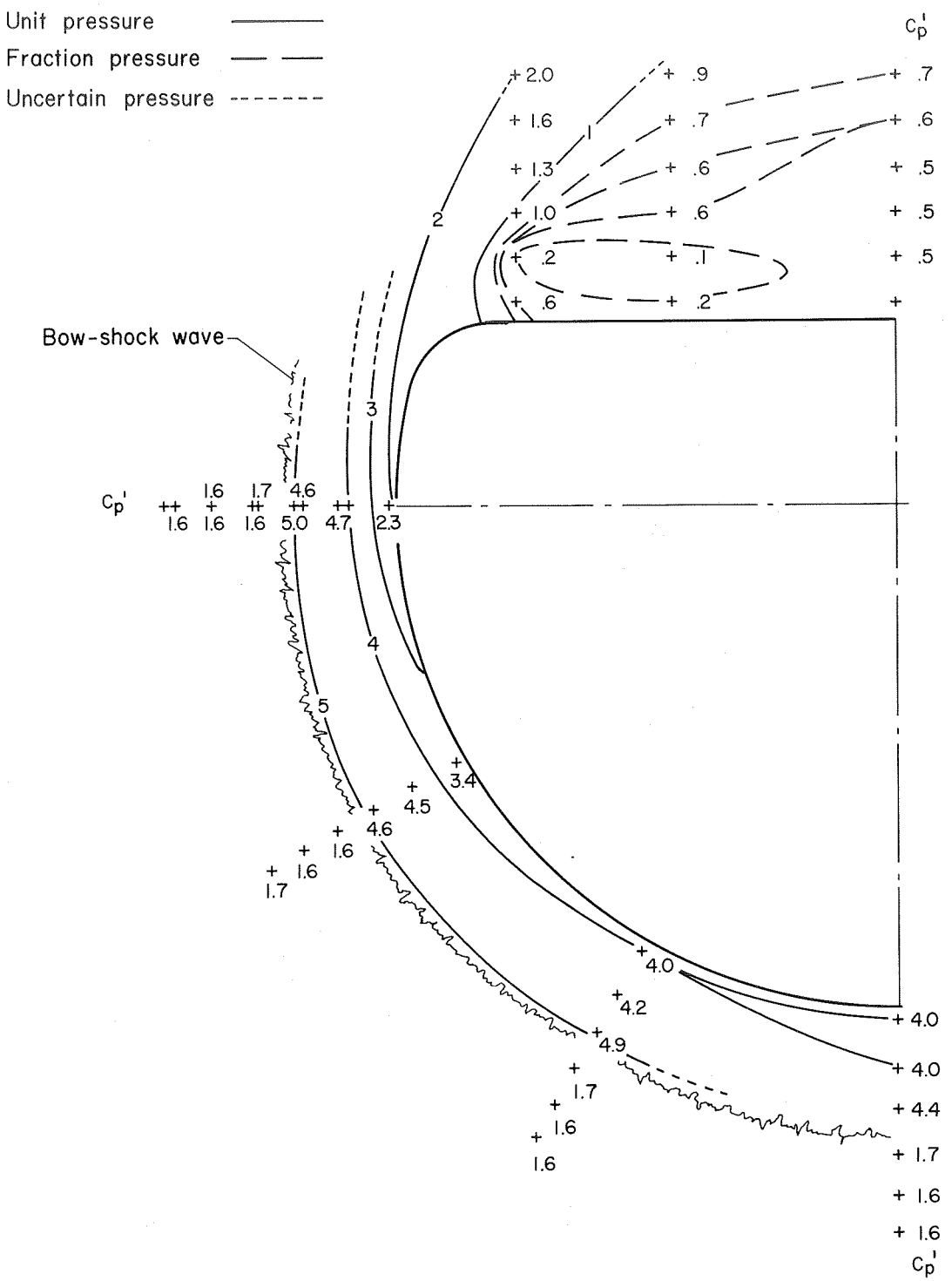

(d) $\alpha = 10^{\circ}$

Figure 19.- Continued.

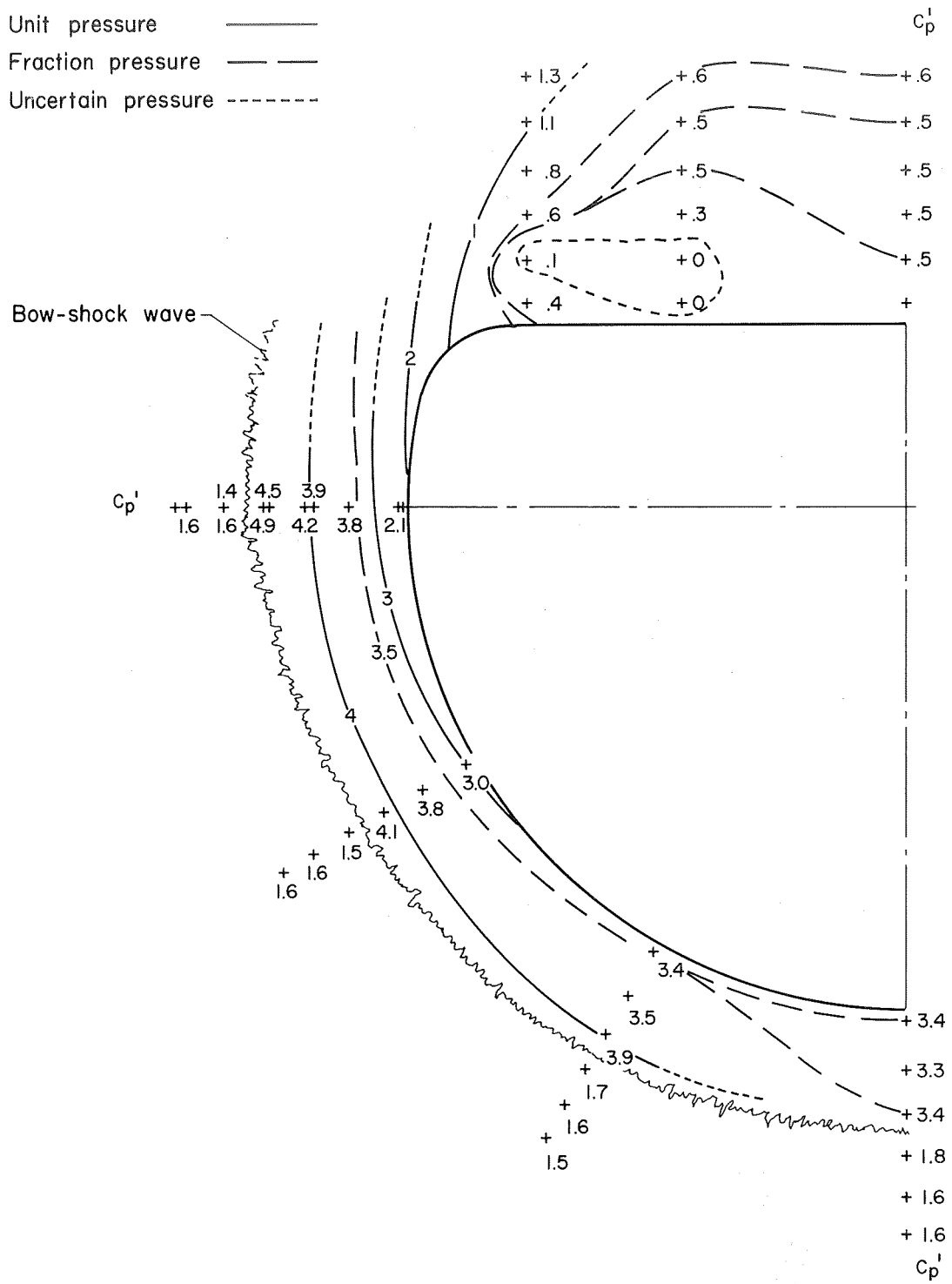

(e) $\alpha = 15^{\circ}$

Figure 19.- Concluded.

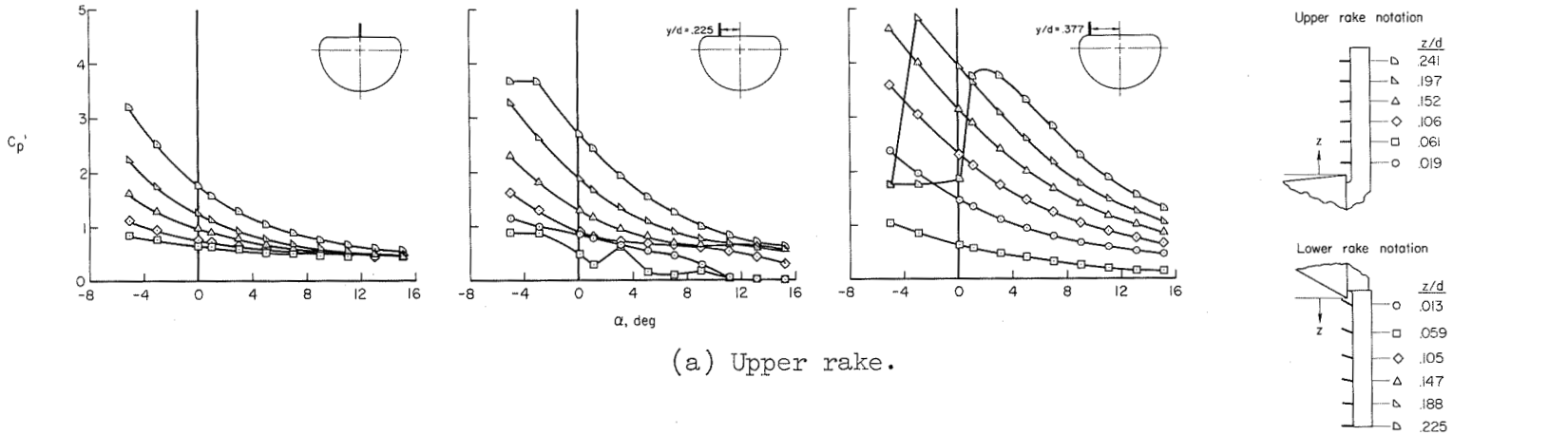

(a) Upper rake.

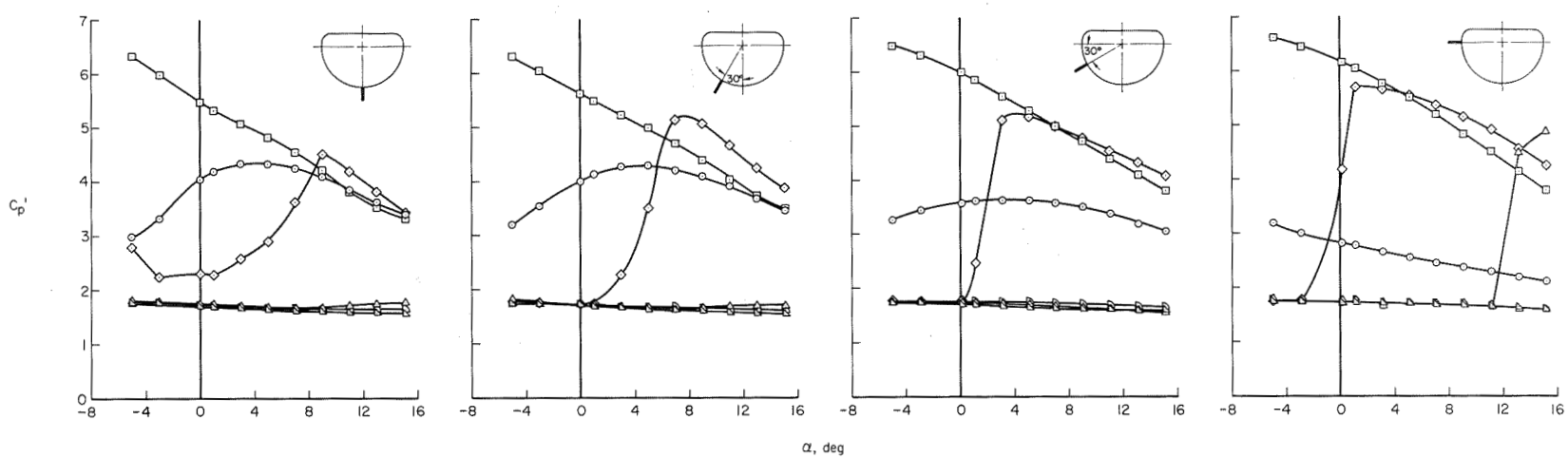

(b) Lower rake.

Figure 20.- Pitot-pressure coefficients in the flow field about the M-1 body at M = 7.4.

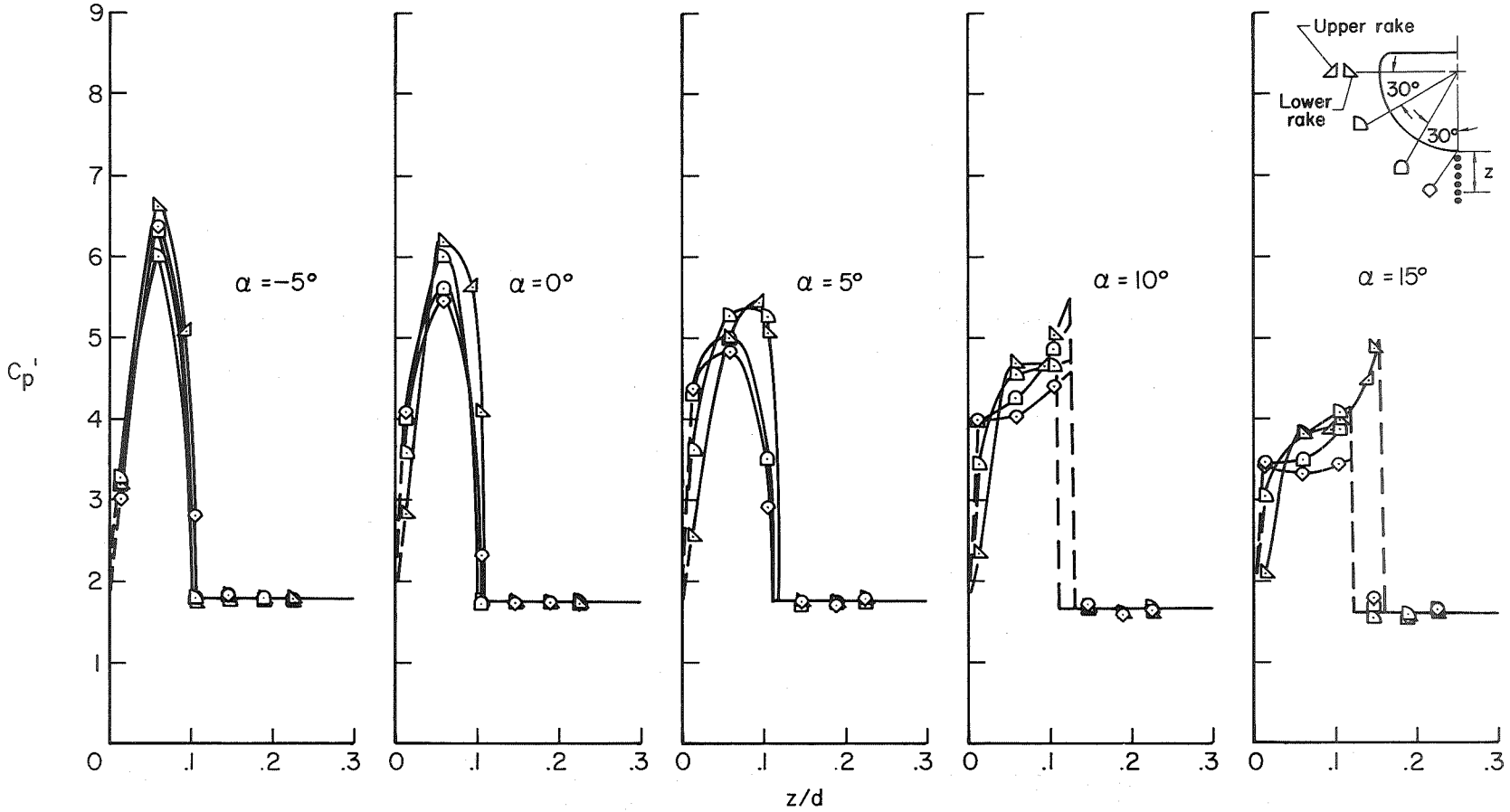

Figure 21.- Pitot-pressure-coefficient profiles through the flow field about the conical surface of the M-1 body at M = 7.4.

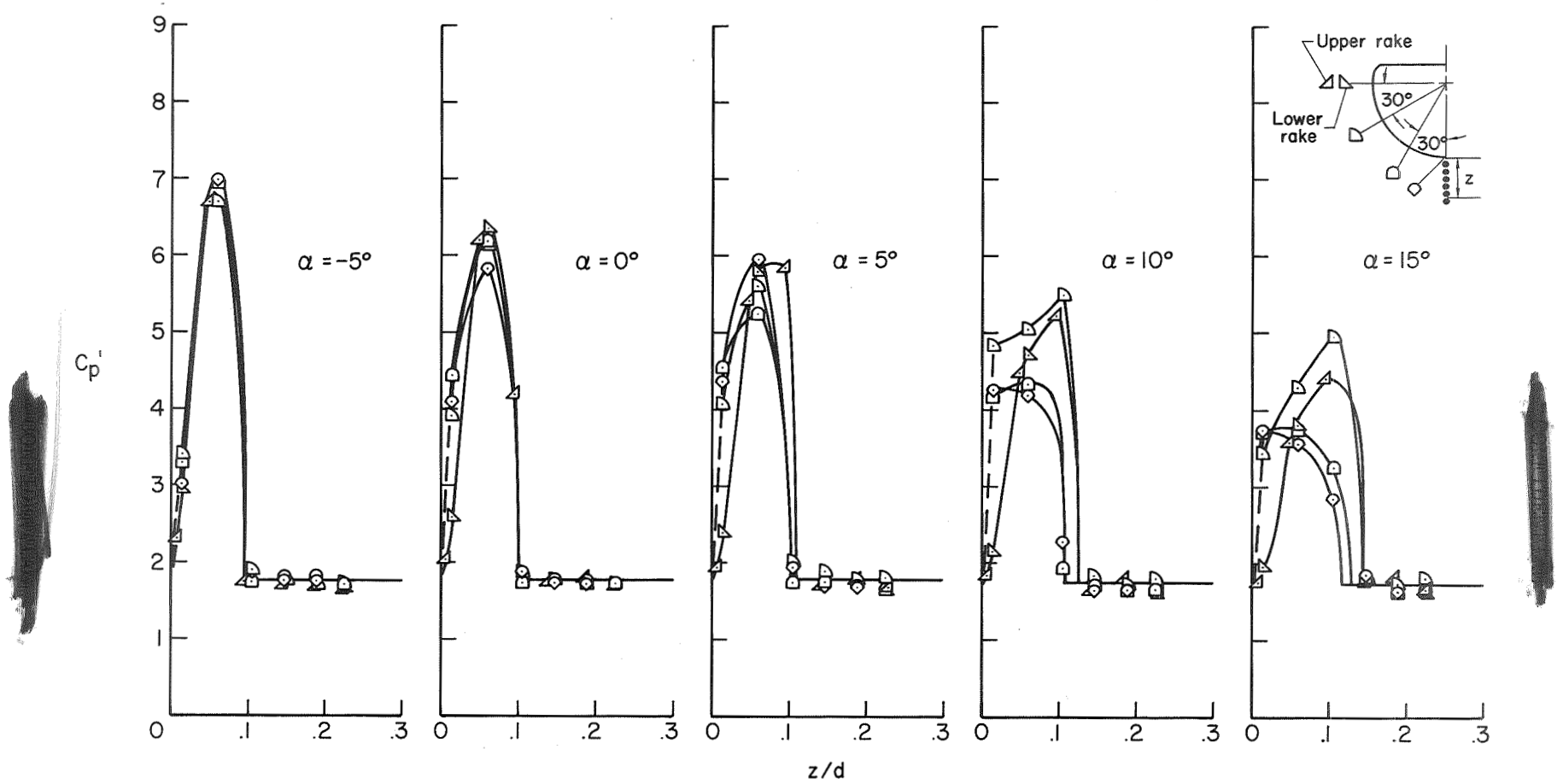

Figure 22.- Pitot-pressure-coefficient profiles through the flow field about the conical surface of the M-1 body at M = 10.4.

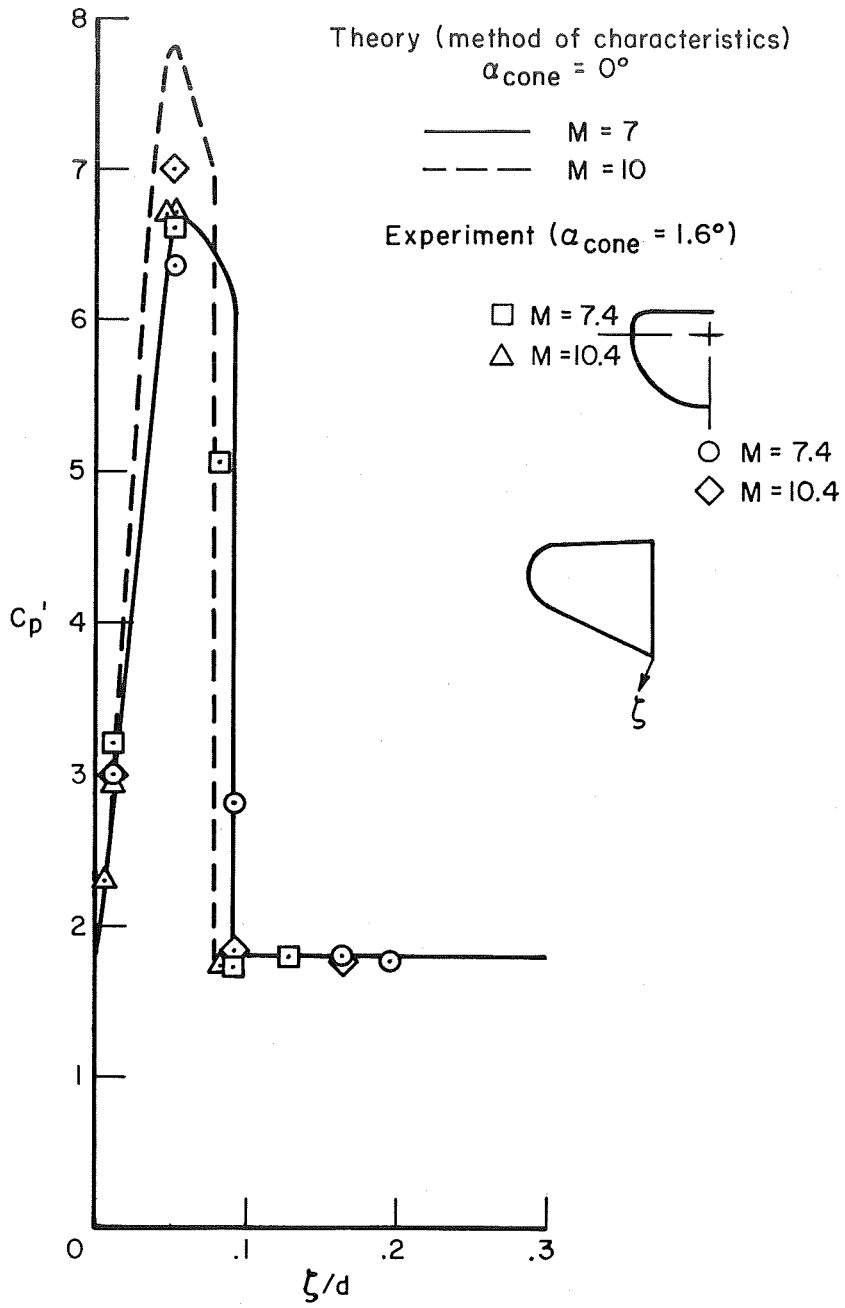

Figure 23.- Pitot-pressure-coefficient profiles normal to the conical surface.

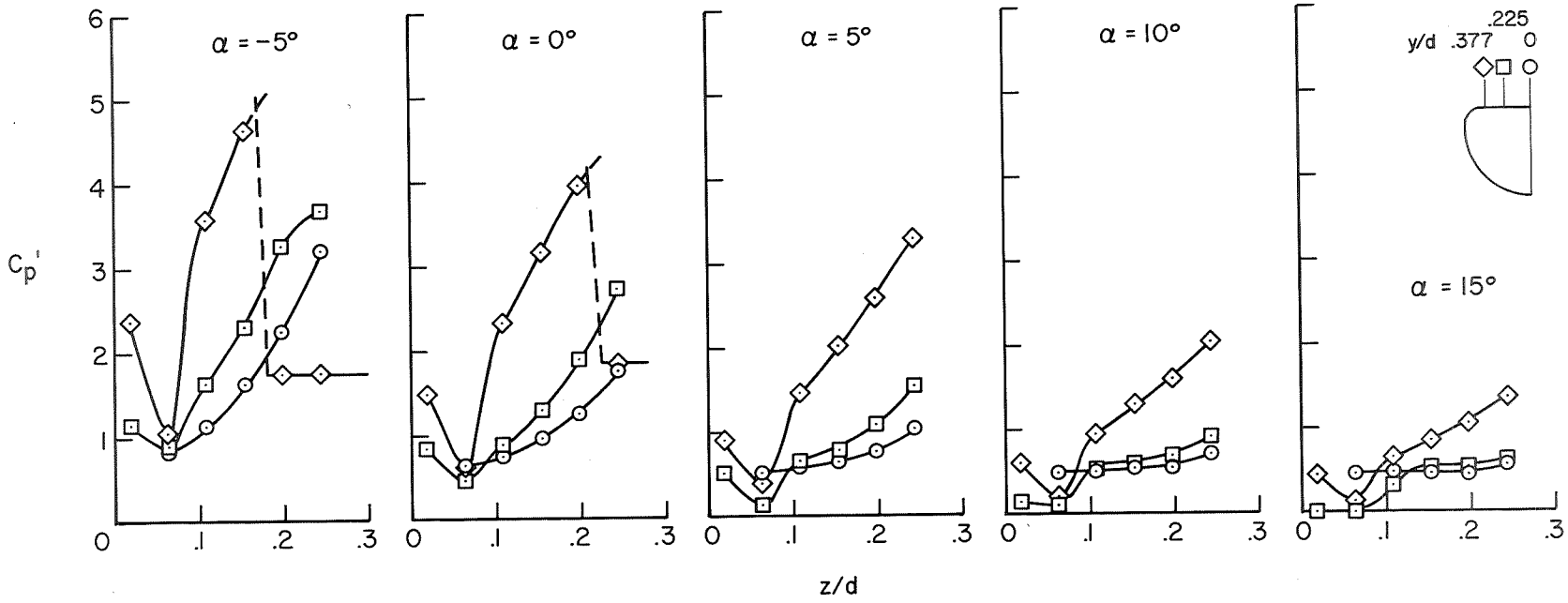

Figure 24.- Pitot-pressure-coefficient profiles through the flow field about the upper surface of the M-1 body at M = 7.4.

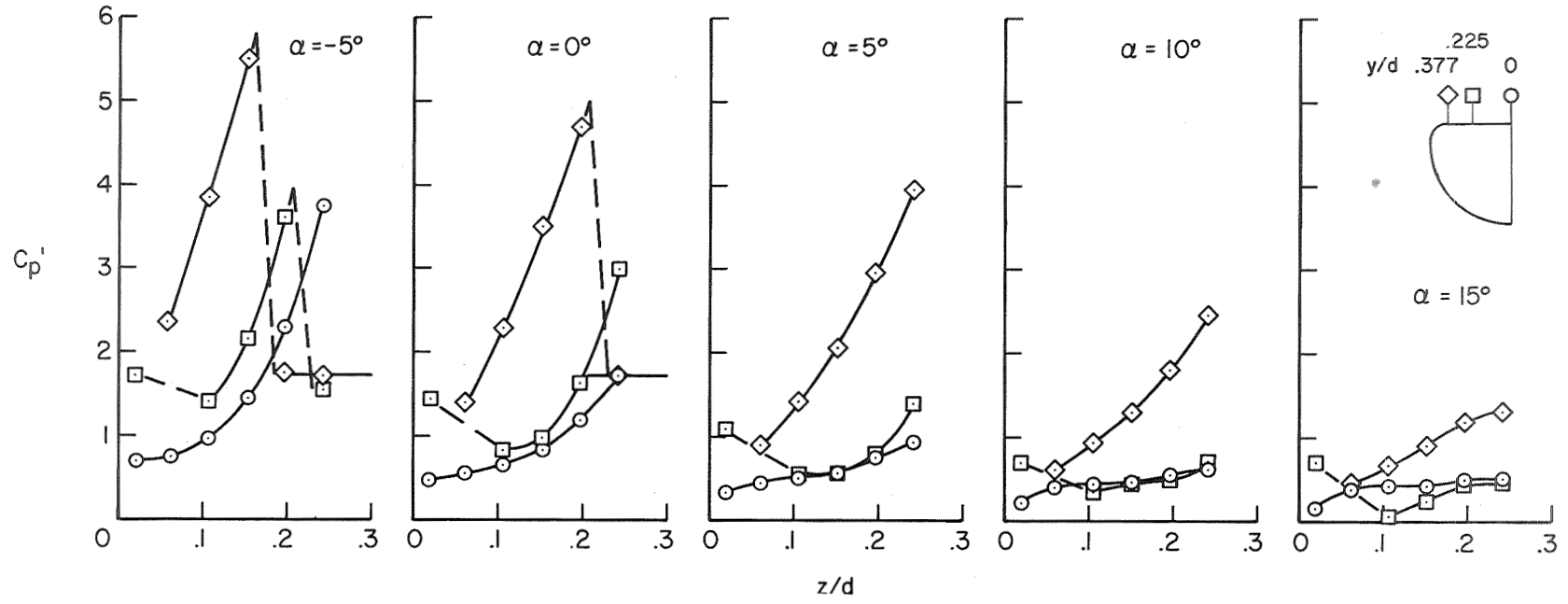

Figure 25.- Pitot-pressure-coefficient profiles through the flow field about the upper surface of the M-1 body at M = 10.4.

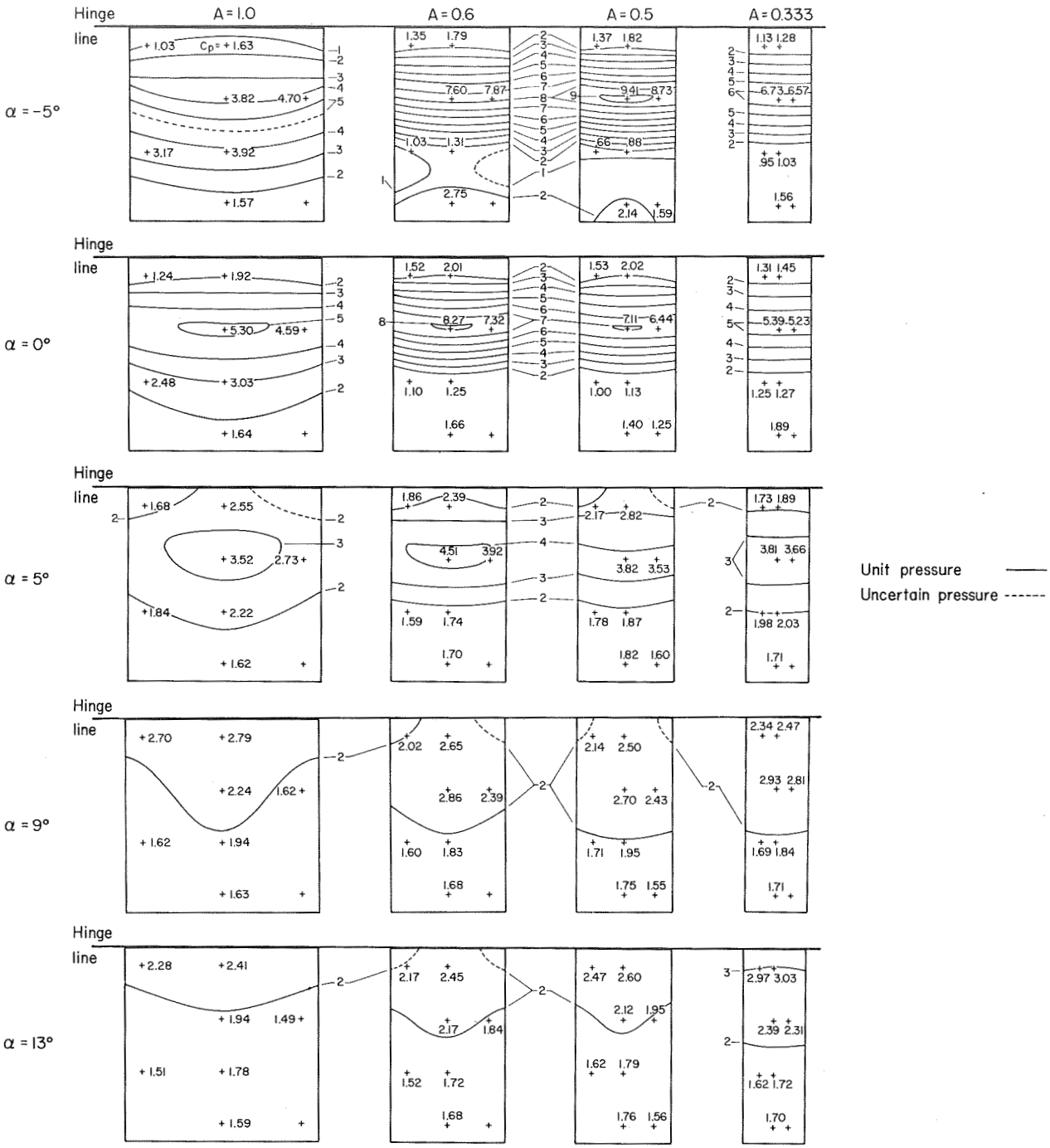

Figure 26.- Isobar diagrams of pressure-coefficient distributions on lower pitch flaps of various output ratios; $\delta_l = 90^\circ$, M = 7.4.

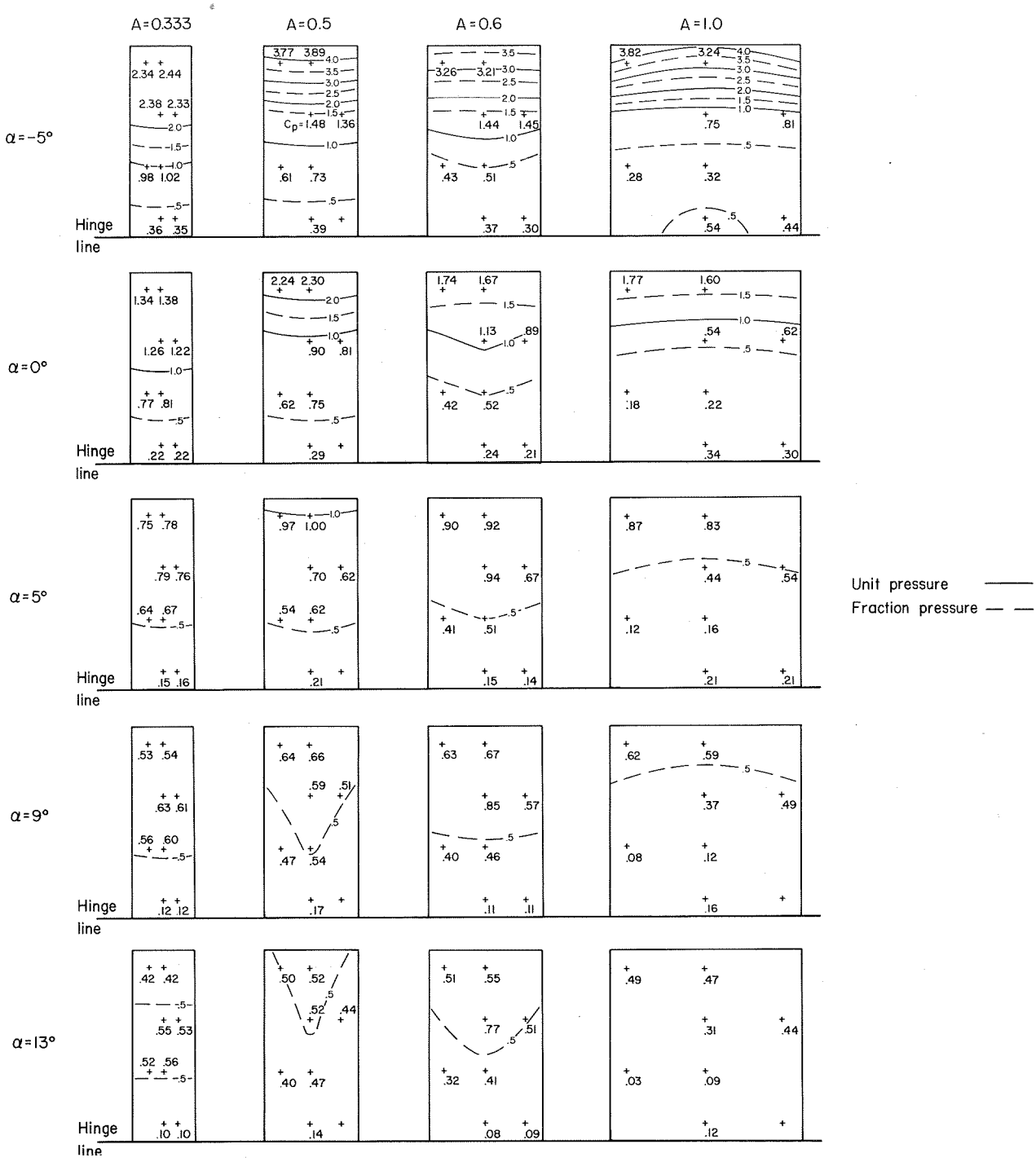

Figure 27.- Isobar diagrams of pressure-coefficient distributions on upper pitch flaps of various aspect ratios; $\delta_u = 90^\circ$, M = 7.4.

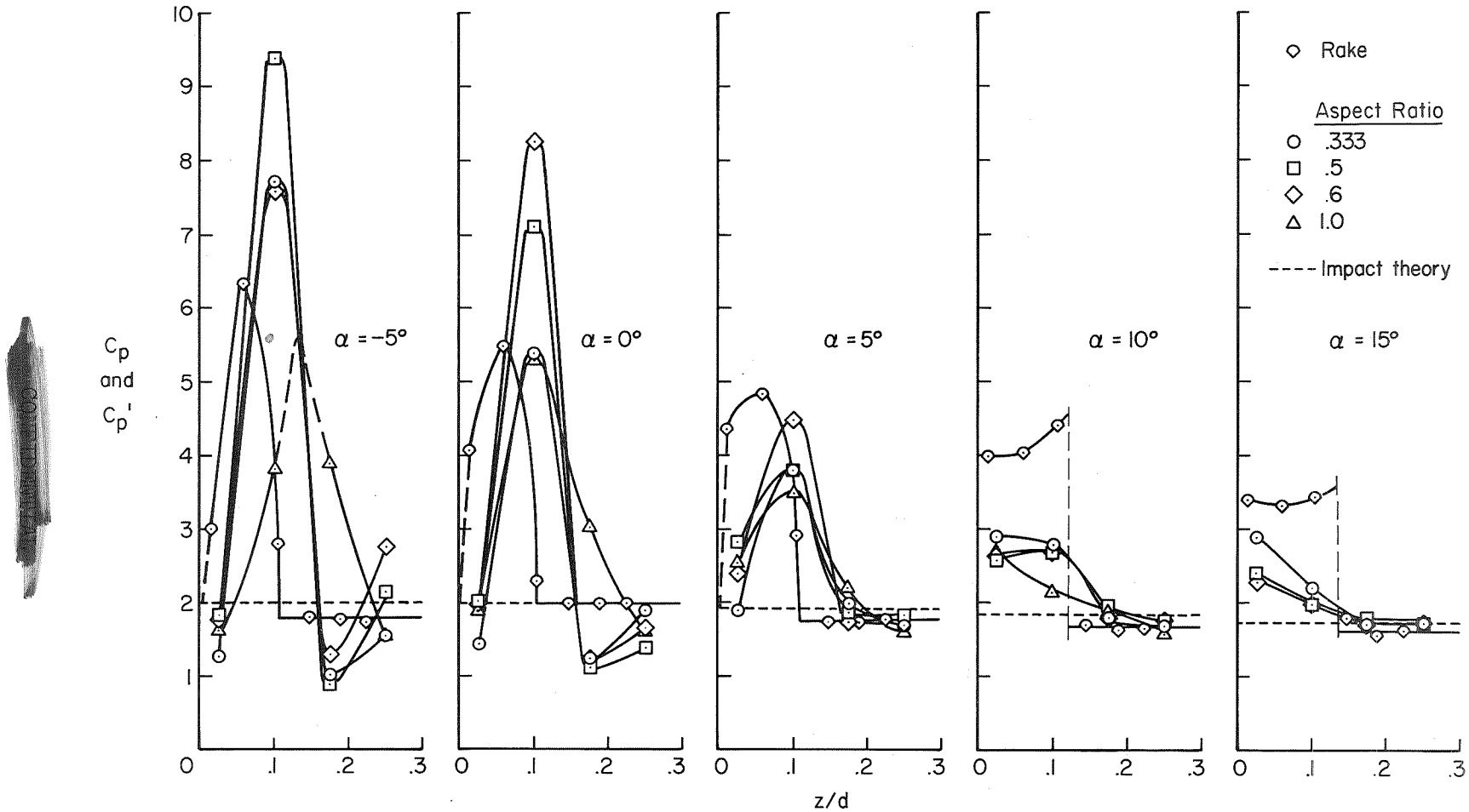

(a) 90° deflection.

Figure 28.- Pressure-coefficient distributions along the center line of lower pitch flaps of various aspect ratios; M = 7.4.

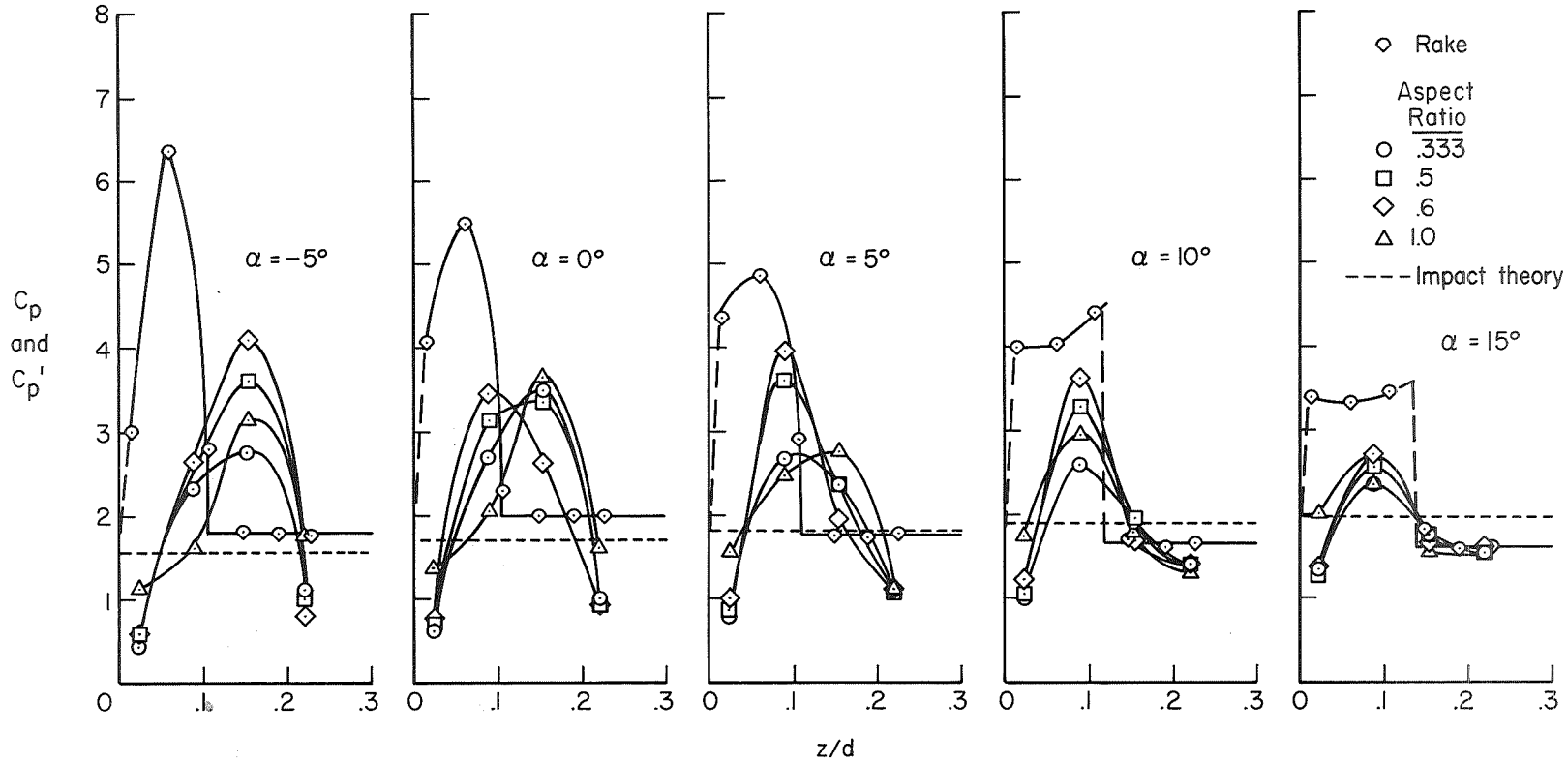

(b) 60° deflection.

Figure 28.- Concluded.

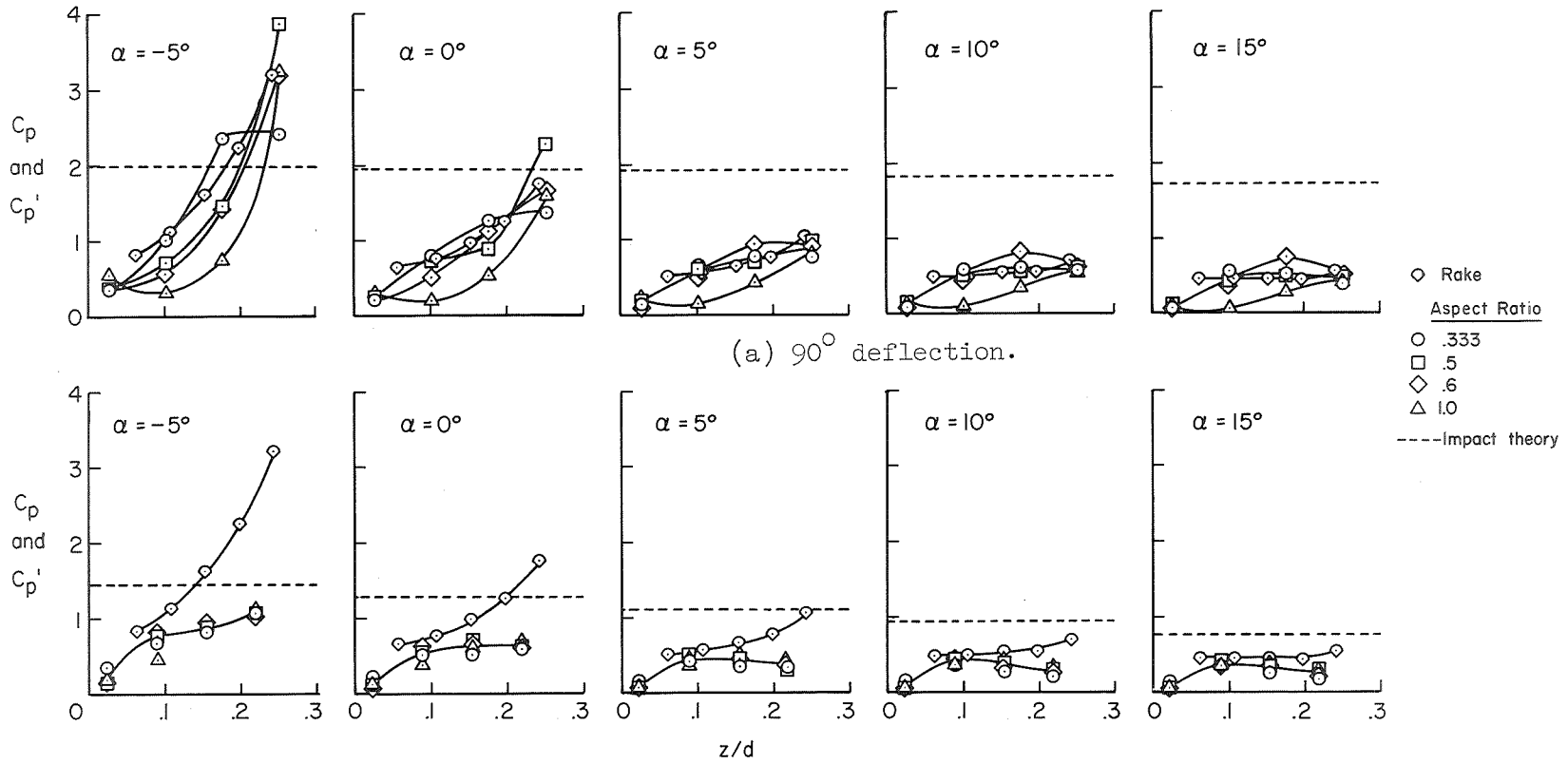

(a) 90° deflection.

(b) 60° deflection.

Figure 29.- Pressure-coefficient distributions along the center line of upper flaps of various aspect ratios; M = 7.4.

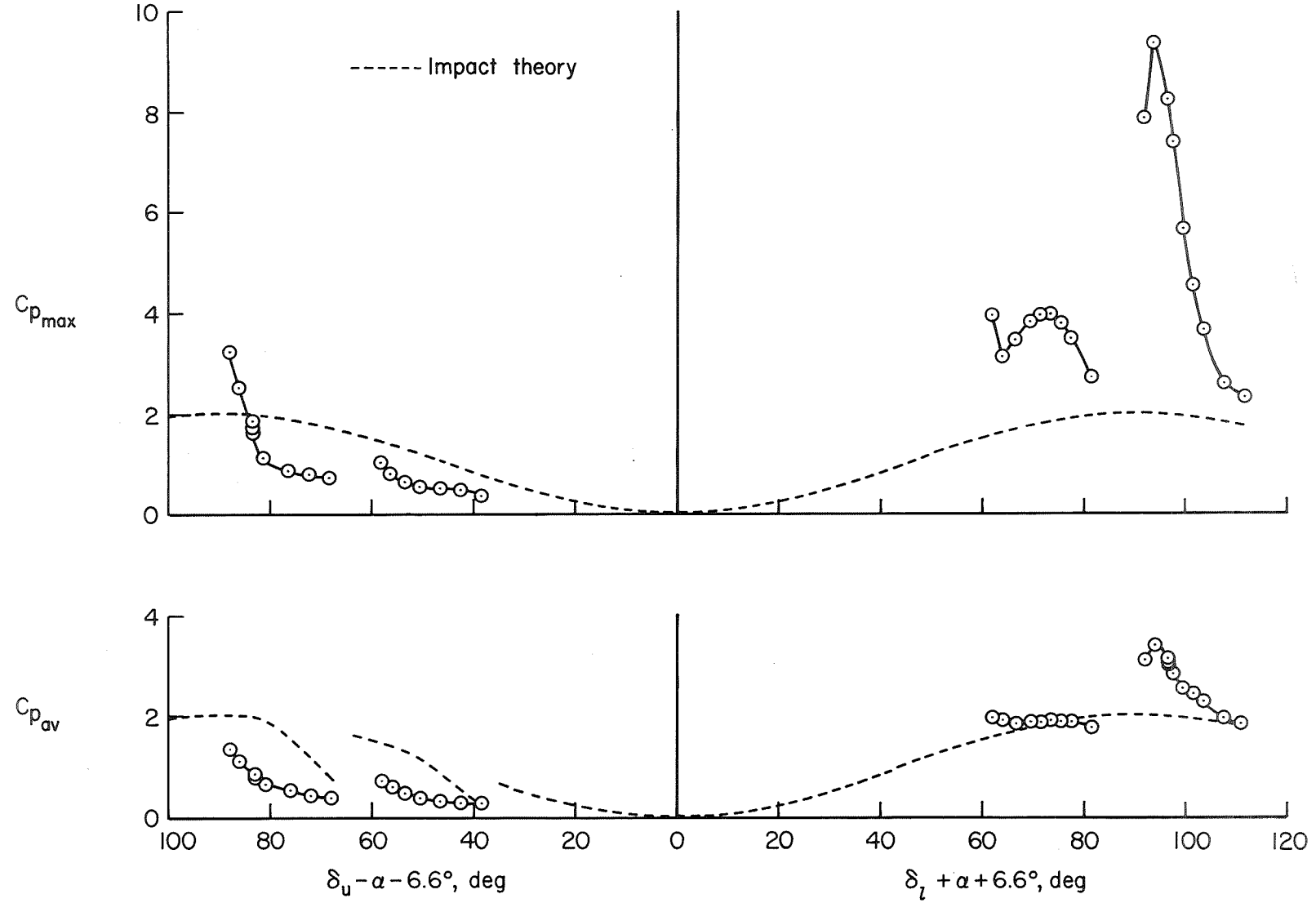

(a) A = 0.6

Figure 30.- Maximum and average pressure coefficients on upper and lower pitch flaps as a function of the angle between the free stream and the flap at M = 7.4.

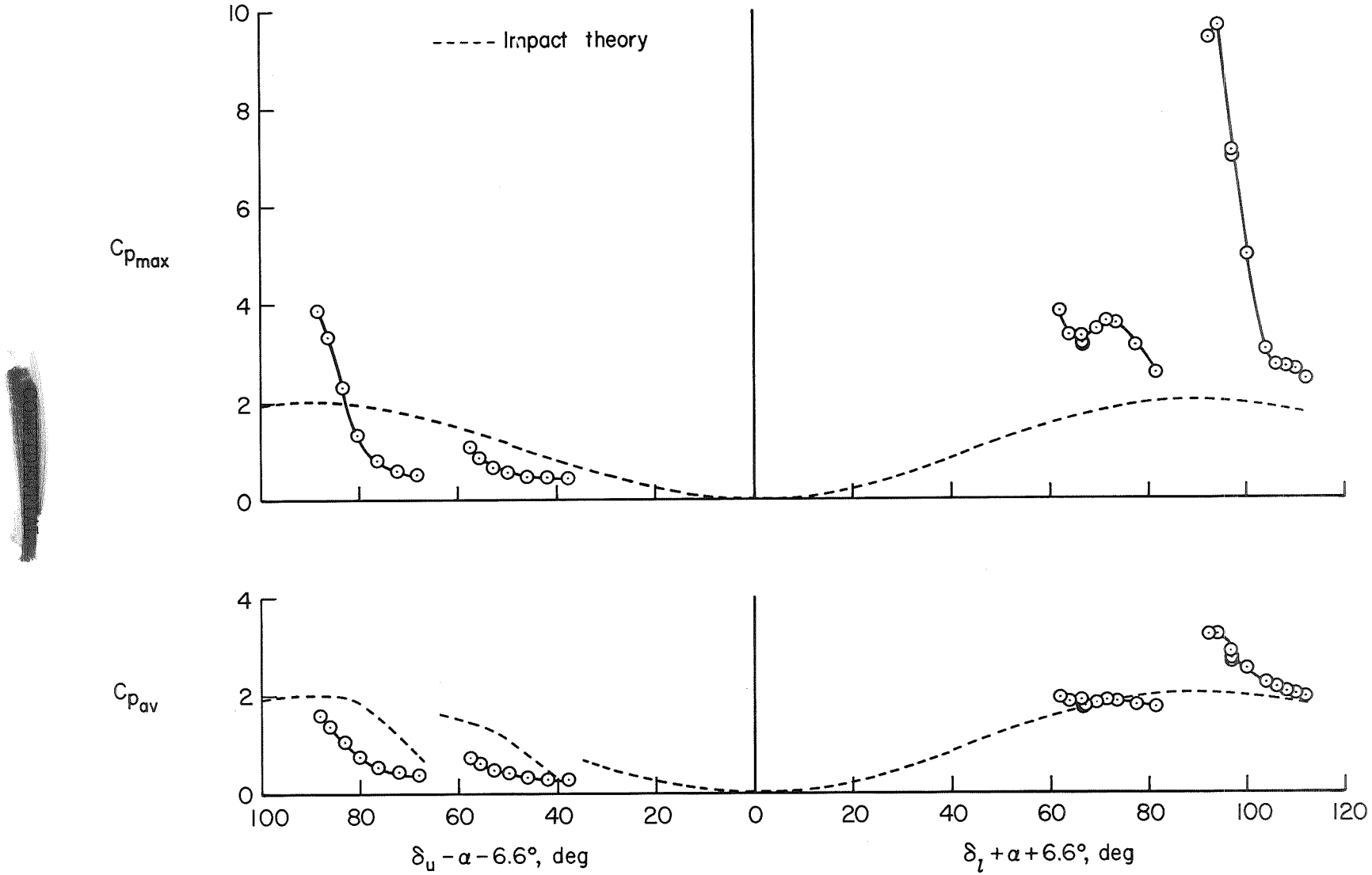

(b) A = 0.5

Figure 30.- Continued.

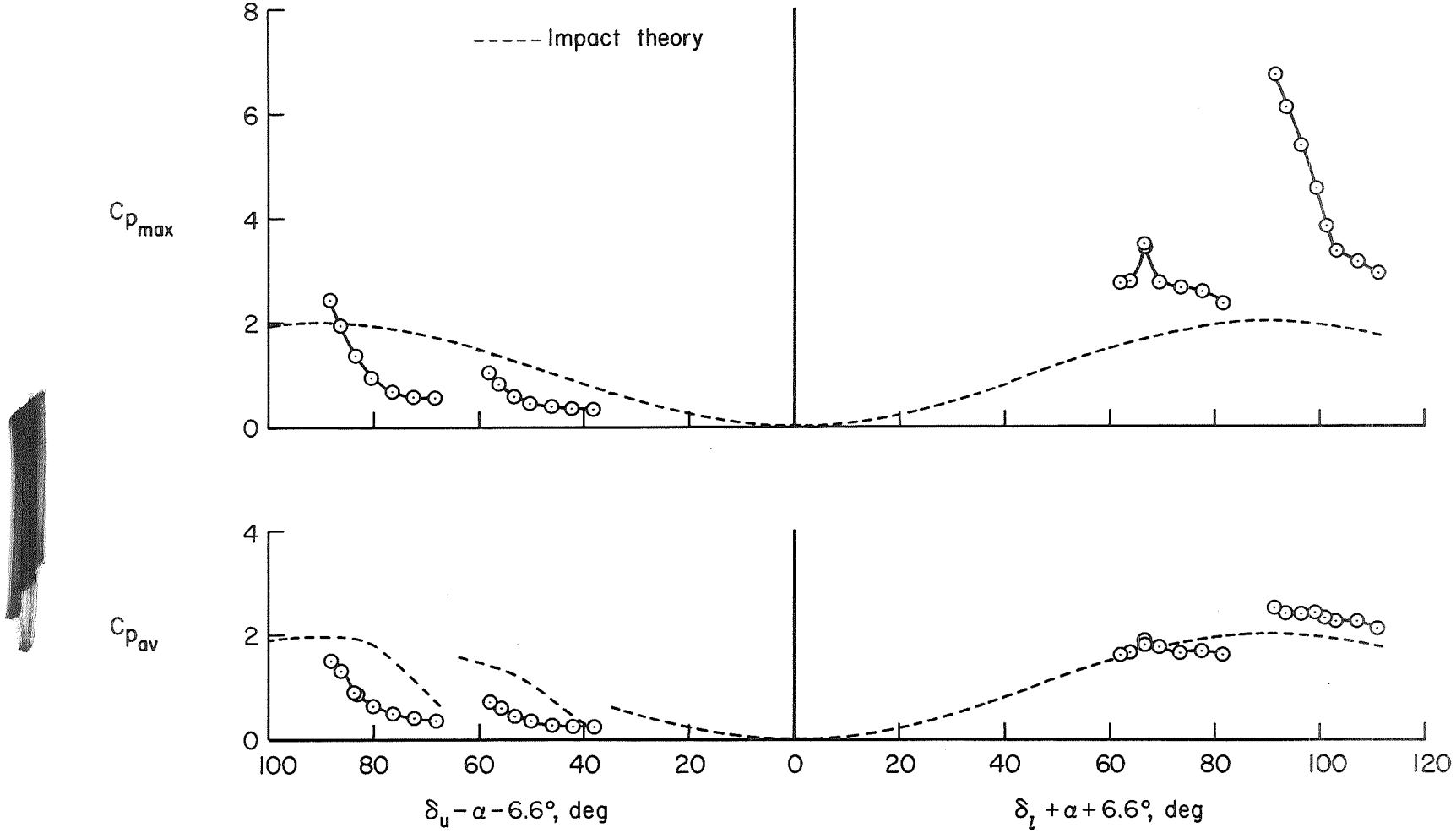

(c) A = 0.333

Figure 30.- Concluded.

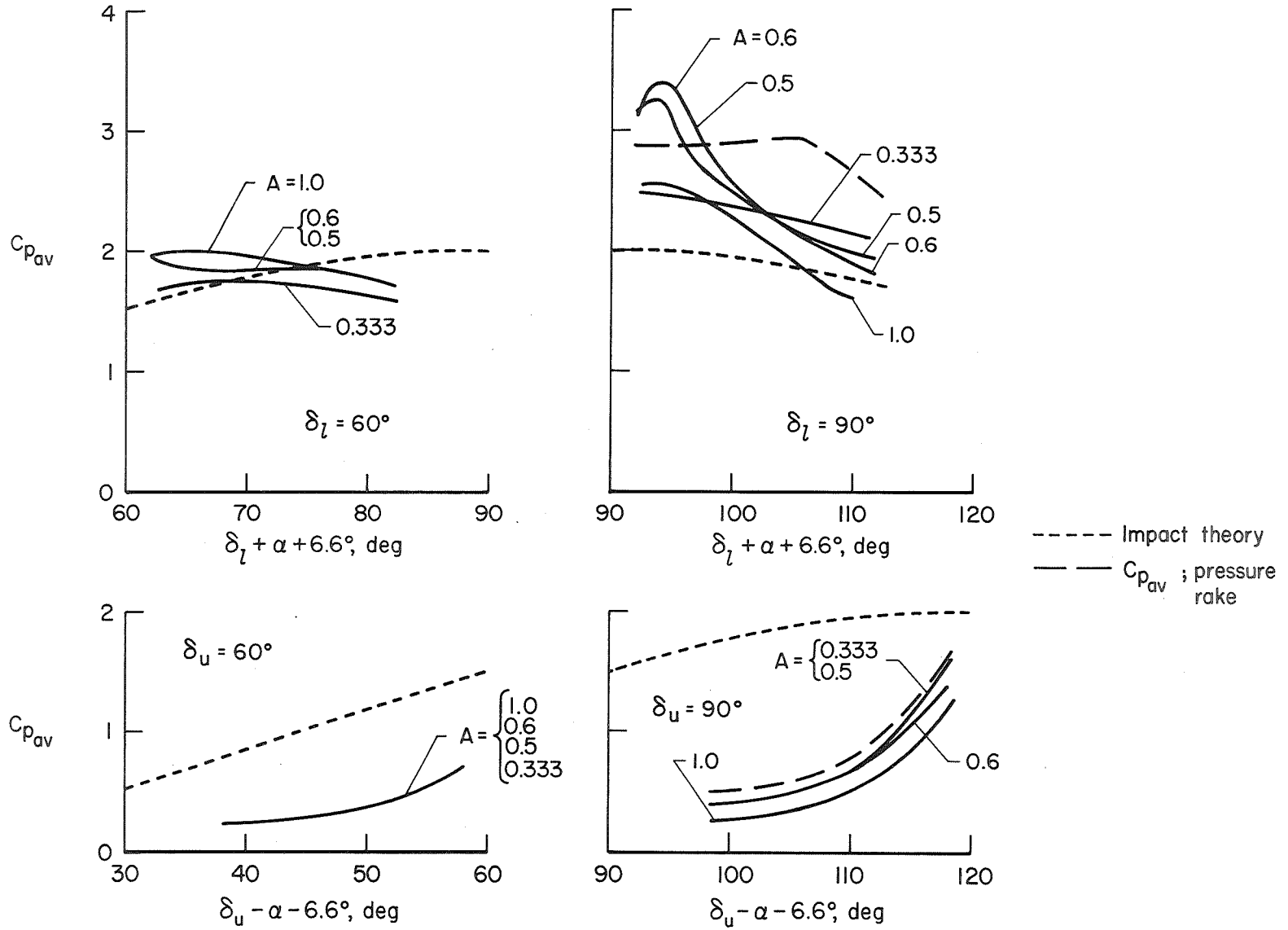

Figure 31.- Average pressure coefficient on upper and lower pitch flaps deflected 60° and 90° for various aspect ratios.

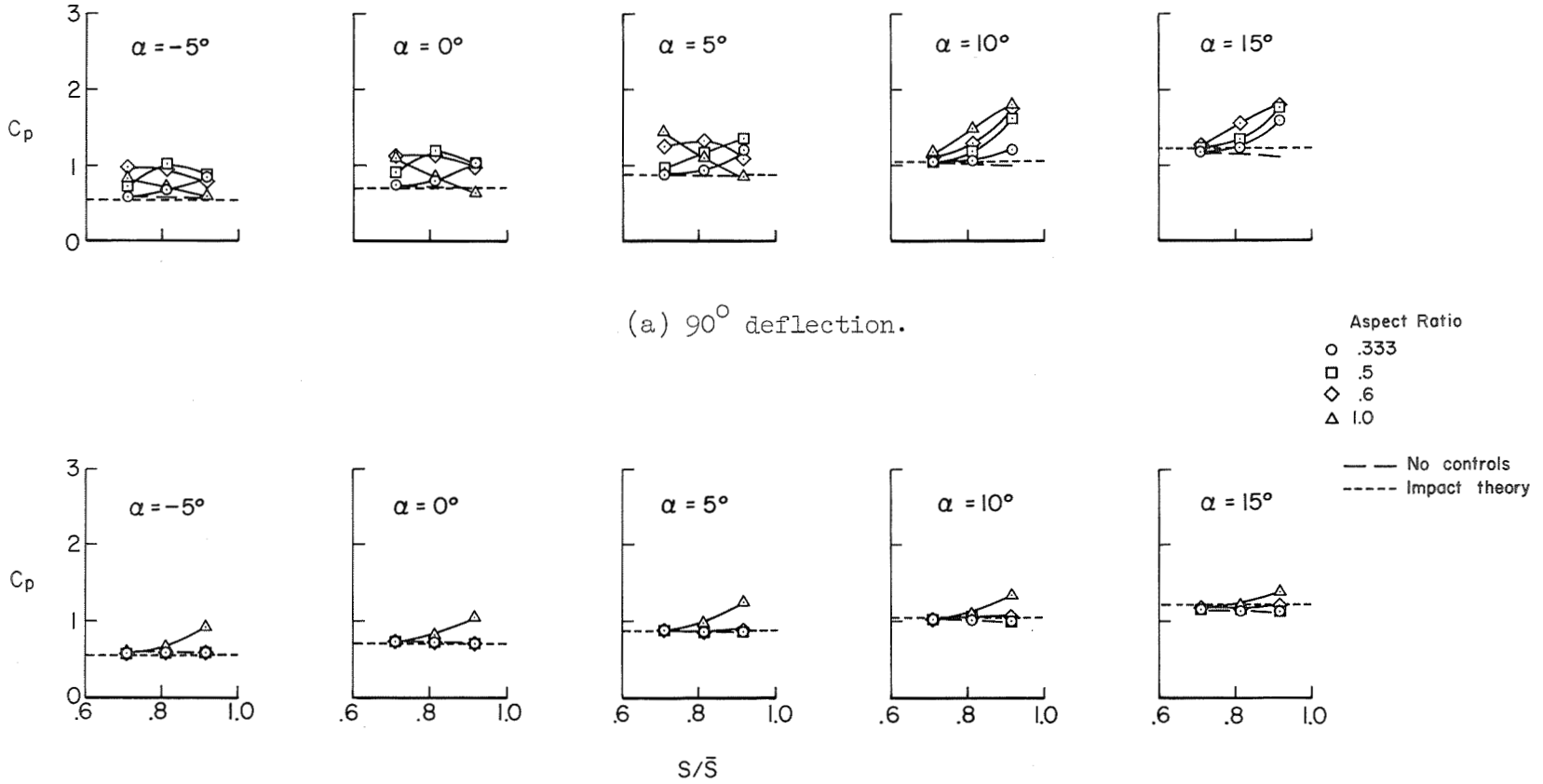

(a) 90° deflection.

(b) 60° deflection.

Figure 32.- Pressure-coefficient distribution on the body upstream from lower flaps of various aspect ratios; M = 7.4.

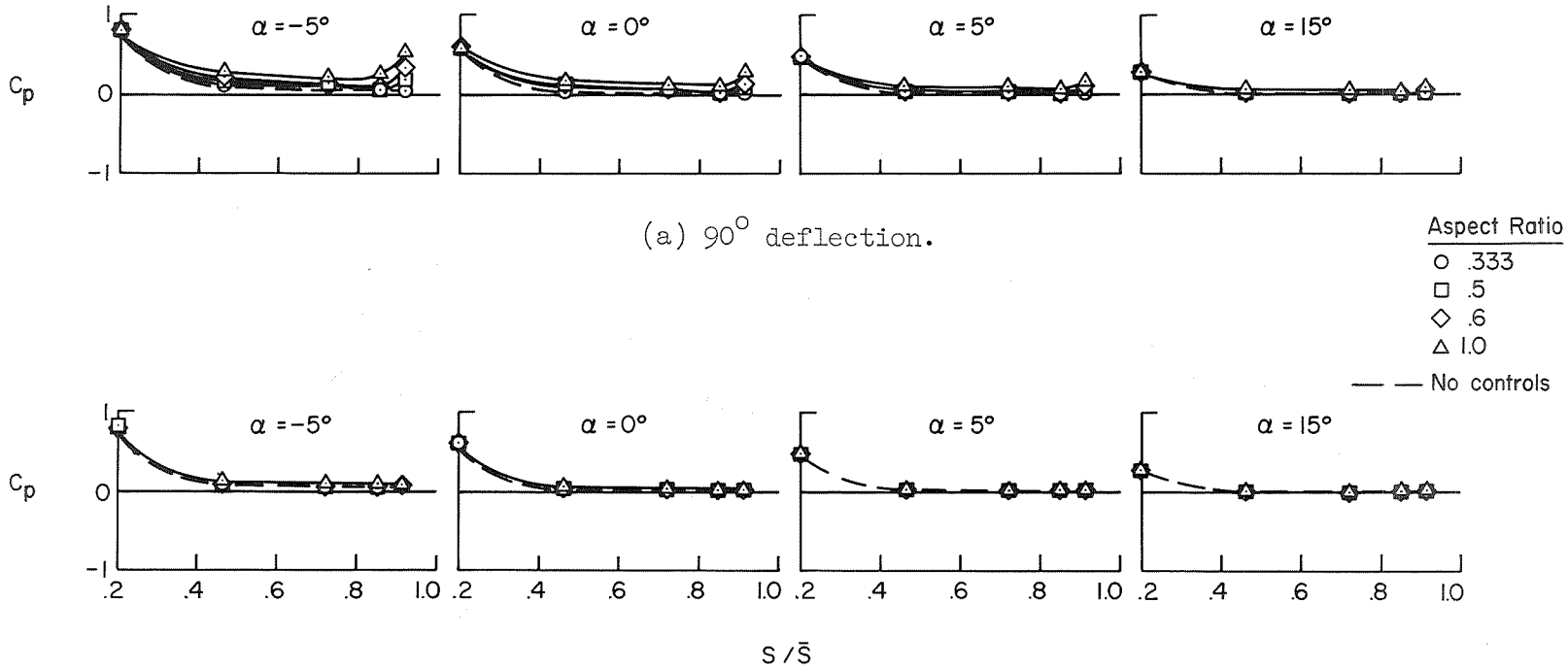

Figure 33.- Pressure-coefficient distribution on the body upstream from upper flaps of various aspect ratios; M = 7.4.

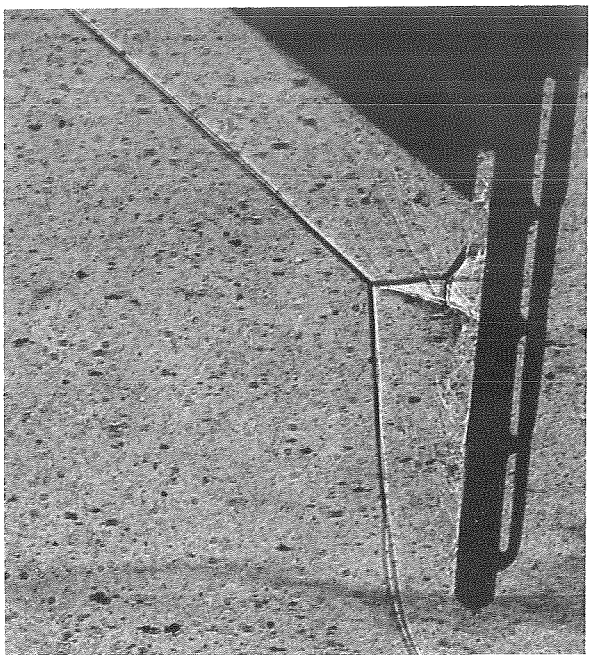

A = 0.333, M = 7.4

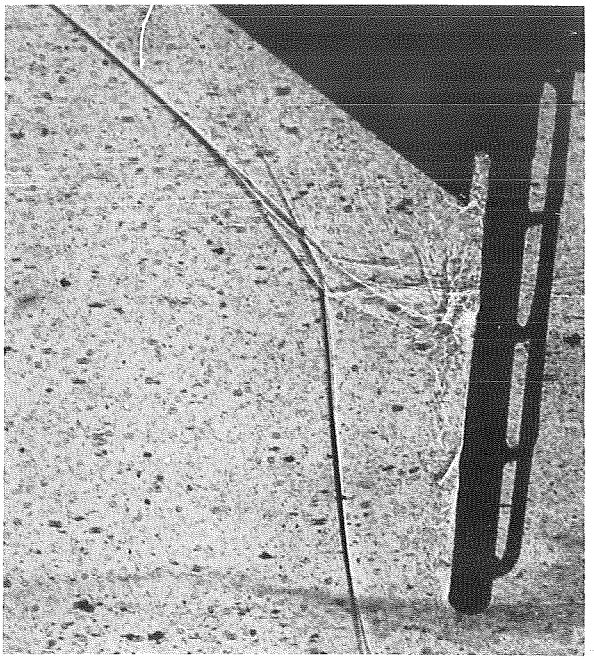

A = 0.5, M = 7.4

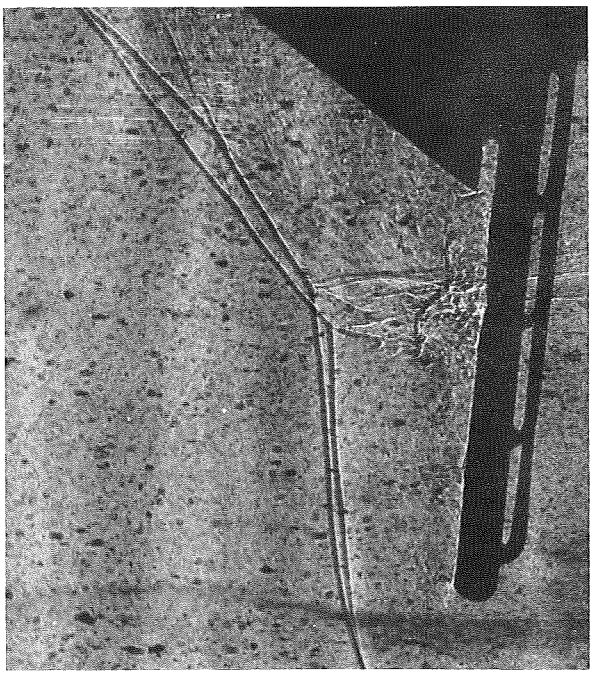

A = 0.6, M = 7.4

Figure 34.- Effect of aspect ratio on the usteady location of shock waves with the lower flap deflected 90° at $\alpha = 0°$ and M = 7.4.

"The aeronautical and space activities of the United States shall be conducted so as to contribute . . . to the expansion of human knowledge of phenomena in the atmosphere and space. The Administration shall provide for the widest practicable and appropriate dissemination of information concerning its activities and the results thereof."

—NATIONAL AERONAUTICS AND SPACE ACT OF 1958

NASA SCIENTIFIC AND TECHNICAL PUBLICATIONS

TECHNICAL REPORTS: Scientific and technical information considered important, complete, and a lasting contribution to existing knowledge.

TECHNICAL NOTES: Information less broad in scope but nevertheless of importance as a contribution to existing knowledge.

TECHNICAL MEMORANDUMS: Information receiving limited distribution because of preliminary data, security classification, or other reasons.

CONTRACTOR REPORTS: Technical information generated in connection with a NASA contract or grant and released under NASA auspices.

TECHNICAL TRANSLATIONS: Information published in a foreign language considered to merit NASA distribution in English.

TECHNICAL REPRINTS: Information derived from NASA activities and initially published in the form of journal articles.

SPECIAL PUBLICATIONS: Information derived from or of value to NASA activities but not necessarily reporting the results of individual NASA-programmed scientific efforts. Publications include conference proceedings, monographs, data compilations, handbooks, sourcebooks, and special bibliographies.

Details on the availability of these publications may be obtained from:

SCIENTIFIC AND TECHNICAL INFORMATION DIVISION

NATIONAL AERONAUTICS AND SPACE ADMINISTRATION

Washington, D.C. 20546